Material Behavior: Texture and Anisotropy

Ralf Hielscher, David Mainprice, and Helmut Schaeben

Contents

R. Hielscher (✉)
Applied Functional Analysis, Technical University Chemnitz, Chemnitz, Germany
e-mail: ralf.hielscher@mathematik.tu-chemnitz.de

D. Mainprice
Géosciences UMR CNRS 5243, Université Montpellier 2, Montpellier, France
e-mail: david.mainprice@gm.univ-montp2.fr

H. Schaeben
Geophysics and Geoinformatics, TU Bergakademie Freiberg, Freiberg, Germany
e-mail: schaeben@tu-freiberg.de

W. Freeden et al. (eds.), *Handbook of Geomathematics*,
DOI 10.1007/978-3-642-54551-1_33

Abstract

This contribution is an attempt to present a self-contained and comprehensive survey of the mathematics and physics of the material behavior of rocks in terms of texture and anisotropy. Being generally multiphase and polycrystalline, where each single crystallite is anisotropic with respect to its physical properties, texture, i.e., the statistical and spatial distribution of crystallographic orientations, becomes a constitutive characteristic and determines material behavior except for grain boundary effects, i.e., in first-order approximation. This chapter is in particular an account of modern mathematical texture analysis explicitly clarifying terms, providing definitions and justifying their application, and emphasizing its major insights. Thus, mathematical texture analysis is brought back to the realm of spherical Radon and Fourier transforms, spherical approximation, and spherical probability, i.e., to the mathematics of spherical tomography.

1 Introduction

Quantitative analysis of crystals' preferred orientation, or texture analysis, is historically important in metallurgy and has become increasingly applied to Earth science problems of the anisotropy of physical properties (e.g., seismic anisotropy) and the study of deformation processes (e.g., plasticity). The orientation probability density function $f : \mathrm{SO}(3) \to \mathbb{R}$, which is used to model the volume portion of crystallites $\mathrm{d}V_g$ realizing a random crystallographic orientation g within a polycrystalline specimen of volume V, is instrumental to the description of the preferred crystallographic orientation, i.e., texture, and to the computation of anisotropic material behavior due to texture. The orientation probability density function can practically be determined (i) from individual orientation measurements (electron backscatter diffraction data) by nonparametric kernel density estimation or (ii) from integral orientation measurements (X-ray, neutron, or synchrotron diffraction data) by resolving the largely ill-posed problem to invert experimentally accessible "pole figure" intensities interpreted as volume portions of crystallites $\mathrm{d}V_{\pm h \| r}$ having the lattice plane normals $\pm\mathbf{h} \in \mathbb{S}^2$ coincide with the specimen direction $\mathbf{r} \in \mathbb{S}^2$. Mathematically, pole density functions are defined in terms of totally geodesic Radon transforms.

Mathematical proofs as well as algorithms and their numerics are generally omitted; instead, the reader is referred to original publications or standard textbooks where they apply, and the new open-source MATLAB®; toolbox "MTEX" for texture analysis, created by Ralf Hielscher (Hielscher and Schaeben 2008a, see also http://code.google.com/p/mtex/), provides a practical numerical implementation of the methods described in the chapter.

References are not meant to indicate or assign priorities; they were rather chosen according to practical reasons, such as accessibility.

2 Scientific Relevance

Several important physical properties of rocks of geophysical interest are controlled by the single-crystal properties of constituent minerals, e.g., thermal conductivity and seismic wave speed. Many minerals have strongly anisotropic mechanical and physical properties; hence, an accurate statistical description of the crystallographic orientation (or texture) of minerals in aggregates of geomaterials is essentially for the prediction of bulk anisotropic properties. Further quantitative texture analysis of minerals provides a means of identifying the minerals that control the anisotropy of rock properties and the deformation mechanisms that generate texture, e.g., dislocation glide systems. The study of crystallographic orientation in rocks dates back to the work of Sander (1930) making measurements with a petrological microscope and interpretation of textures in terms of rock movement or flow patterns in the 1920s. Hence, it has been recognized for a long time that texture records important information of the history or evolution of a rock, which may reflect on past conditions of temperature, pressure, and mechanical deformation. Recent advances have extended the field of texture analysis from naturally deformed specimens found on the surface to samples experimentally deformed at the high pressures of the Earth's mantle. Mainprice et al. (2005) and core Mao et al. (1998), corresponding to depths of hundreds or thousands of kilometers below the Earth's surface. Texture analysis is an important tool for understanding the deformation behavior of experimentally deformed samples. New diffraction techniques using synchrotron high-intensity X-ray radiation on micron-sized high-pressure samples (Raterron and Merkel 2009) and the now widespread application of electron backscatter diffraction (EBSD) to a diverse range of geological samples (Prior et al. 2009) require a modern texture analysis that can be coherently applied to volume diffraction data, single orientation measurements, and plasticity-modeling schemes involving both types of data. The texture analysis proposed in this chapter constitutes a reply to these new requirements within a rigorous mathematical framework.

3 Rotations and Crystallographic Orientations

The special orthogonal group SO(3) is initially defined as the group of rotations $g \in \mathbb{R}^{3\times3}$ with $\det(g) = +1$. It may be characterized as a differentiable manifold and endowed with a metric and a distance as a Riemannian manifold (Morawiec 2004).

An orientation is defined to mean an instantaneous rotational configuration. Let $\mathcal{K}_S = \{\mathbf{x}, \mathbf{y}, \mathbf{z}\}$ be a right-handed orthonormal specimen coordinate system, and let $\mathcal{K}_C = \{\mathbf{a}, \mathbf{b}, \mathbf{c}\}$ be a right-handed orthonormal crystal coordinate system. Then, we call the rotation $g \in \mathrm{SO}(3)$ of the coordinate system $\mathcal{K}_C$ with respect to the coordinate system $\mathcal{K}_S$ if it rotates the latter onto the former system, i.e., if $g\mathbf{x} = \mathbf{a}, g\mathbf{y} = \mathbf{b}, \mathbf{g}z = \mathbf{c}$. Let $\mathbf{r} = (u, v, w)^T$ be a unit coordinate vector with respect to the

specimen coordinate system $\mathcal{K}_S$, and let $\mathbf{h} = (h, k, l)^T$ be the corresponding unit coordinate vector with respect to the crystallographic coordinate system $\mathcal{K}_C$, i.e., both coordinate vectors represent the same direction such that

$$u\mathbf{x} + v\mathbf{y} + w\mathbf{z} = h\mathbf{a} + k\mathbf{b} + l\mathbf{c}.$$

Then, the orientation $g \in \mathrm{SO}(3)$ identified with a matrix $M(g) \in \mathbb{R}^{3\times 3}$ realizes the basis transformation between the coordinate systems, and we have

$$M(g)\mathbf{h} = \mathbf{r}.$$

Casually, $\mathbf{h} \in \mathbb{S}^2$ is referred to as crystallographic direction, while $\mathbf{r} \in \mathbb{S}^2$ is referred to as specimen direction.

Initially, a crystallographic orientation should be thought of as an element $g \in \mathrm{O}(3)$, the orthogonal group. Considering crystallographic symmetries, mathematically different orientations of a crystal may be physically equivalent. The set of all orientations that are equivalent to the identical orientation $g_0 = \mathrm{id}$ is called the point group S_{point} of the crystal. With this notation, the set of all orientations crystallographically symmetrically equivalent to an arbitrary orientation $g_0 \in \mathrm{O}(3)$ becomes the left coset $g_0 S_{\mathrm{point}} = \{g_0 g | g \in S_{\mathrm{point}}\}$. The set of all these cosets is denoted $\mathrm{O}(3)/S_{\mathrm{point}}$ and called quotient orientation space, i.e., the orientation space modulo crystallographic symmetry S_{point}.

In case of diffraction experiments, not only this crystallographic equivalence but also equivalence imposed by diffraction itself has to be considered. Due to Friedel's law (Friedel 1913), equivalence of orientations with respect to diffraction is described by the Laue group S_{Laue}, which is the point group of the crystal augmented by inversion, i.e., $S_{\mathrm{Laue}} = S_{\mathrm{point}} \otimes \{\mathrm{id}, -\mathrm{id}\}$. Since $\mathrm{O}(3)/S_{\mathrm{Laue}} \cong \mathrm{SO}(3)/(S_{\mathrm{Laue}} \cap \mathrm{SO}(3))$, the cosets of equivalent orientations with respect to diffraction are completely represented by proper rotations.

Likewise, when analyzing diffraction data for a preferred crystallographic orientation, it is sufficient to consider the restriction of the Laue group $G_{\mathrm{Laue}} \subset \mathrm{O}(3)$ to its purely rotational part $\tilde{G}_{\mathrm{Laue}} = G_{\mathrm{Laue}} \cap \mathrm{SO}(3)$. Then, two orientations $g, g' \in \mathrm{SO}(3)$ are called crystallographically symmetrically equivalent with respect to $\tilde{G}_{\mathrm{Laue}}$ if there is a symmetry element $q \in \tilde{G}_{\mathrm{Laue}}$ such that $gq = g'$. The left cosets $g\tilde{G}_{\mathrm{Laue}}$ define the classes of crystallographically symmetrically equivalent orientations. Thus, a crystallographic orientation is a left coset. These cosets define a partition of SO(3). A set of class representatives, that contains exactly one element of each left coset or class is called a left transversal. It is not unique. If it is easily tractable with respect to a parametrization, it will be denoted $\mathbb{G}$.

Analogously, two crystallographic directions $\mathbf{h}, \mathbf{h}' \in \mathbb{S}^2$ are called crystallographically symmetrically equivalent if there is a symmetry element $q \in \tilde{G}_{\mathrm{Laue}}$ such that $q\mathbf{h} = \mathbf{h}'$.

The orientation probability density function f of a polycrystalline specimen is defined as $f\colon \mathrm{SO}(3) \to \mathbb{R}$, which models the relative frequencies of crystallographic

orientations within the specimen by volume, i.e., $f(g)dg = \frac{\mathrm{d}V_g}{V}$, and is normalized to

$$\int_{\mathrm{SO}(3)} f(g)dg = 8\pi^2, \tag{1}$$

where dg denotes the rotational invariant measure on SO(3). The orientation probability density function possesses the symmetry property

$$f(g) = f(gq), \quad g \in \mathrm{SO}(3),\ q \in \tilde{G}_{\mathrm{Laue}}, \tag{2}$$

i.e., it is essentially defined on the quotient space $\mathrm{SO}(3)/\tilde{G}_{\mathrm{Laue}}$.

Crystallographic preferred orientations may also be represented by the pole density function $P : \mathbb{S}^2 \times \mathbb{S}^2 \to \mathbb{R}$, where $P(\mathbf{h},\mathbf{r})$ models the relative frequencies that a given crystallographic direction or any crystallographically symmetrically equivalent direction or its antipodally symmetric direction $\pm\mathbf{h} \in \mathbb{S}^2$ coincides with a given specimen direction $\mathbf{r} \in \mathbb{S}^2$, i.e., $P(\mathbf{h},\mathbf{r})d\mathbf{h} = P(\mathbf{h},\mathbf{r})d\mathbf{r} = \frac{\mathrm{d}V_{\pm\mathbf{h}\|\mathbf{r}}}{V}$, and is normalized to

$$\int_{\mathbb{S}^2} P(\mathbf{h},\mathbf{r})\mathrm{d}\mathbf{h} = \int_{\mathbb{S}^2} P(\mathbf{h},\mathbf{r})\mathrm{d}\mathbf{r} = 4\pi.$$

Thus, it satisfies the symmetry relationships

$$P(\mathbf{h},\mathbf{r}) = P(-\mathbf{h},\mathbf{r}) \text{ and } P(\mathbf{h},\mathbf{r}) = P(q\mathbf{h},\mathbf{r}), \quad \mathbf{h},\mathbf{r} \in \mathbb{S}^2,\ q \in \tilde{G}_{\mathrm{Laue}},$$

i.e., it is essentially defined on $\mathbb{S}^2/S_{\mathrm{Laue}} \times \mathbb{S}^2$. Pole density functions are experimentally accessible as "pole figures" by X-ray, neutron, or synchrotron diffraction for some crystallographic forms $\mathbf{h}$, i.e., crystallographic directions and their crystallographically symmetrical equivalents. Orientation probability density and pole density functions are related to each other by the totally geodesic Radon transform.

3.1 Parametrizations and Embeddings

Parametrizations are a way of describing rotations in a quantitative manner. The two major parametrizations we shall consider are the intuitively most appealing parametrization of a rotation in terms of its angle $\omega \in [0,\pi]$ and axis $\mathbf{n} \in \mathbb{S}^2$ of rotation and the parametrization in terms of Euler angles (α,β,γ), with $\alpha,\gamma \in [0,2\pi)$ and $\beta \in [0,\pi]$.

Of particular interest are the embeddings of rotations in $\mathbb{R}^{3\times3}$ or in $\mathbb{S}^3 \subset \mathbb{H}$, the skew field of real quaternions Altmann 1986; Gürlebeck and Sprößig (1997); Hanson 2006; Kuipers 1999.

The eigenvalues of a rotation matrix $M(g) \in \mathbb{R}^{3\times 3}$ are given by $\lambda_1 = 1$ and $\lambda_{2,3} = e^{\pm i\omega}$, where $0 \leq \omega \leq \pi$. The argument ω of the eigenvalues $\lambda_{2,3}$ of a rotation matrix $M(g)$ can be uniquely determined by

$$\operatorname{trace}(M(g)) = 1 + 2\cos\omega,$$

which defines the angle of rotation ω. Furthermore, the axis $\mathbf{n} \in \mathbb{S}^2$ of an arbitrary rotation given as a matrix with entries $M(g) = (m_{i,j})_{i,j=1,\dots,3} \in \mathbb{R}^{3\times 3}$, with $M(g) \neq I_3$, is defined to be

$$\mathbf{n} = \frac{1}{2\sin\omega}(m_{23} - m_{32}, m_{31} - m_{13}, m_{12} - g_{21})^{\mathrm{T}},$$

where $0 < \omega \leq \pi$ is the rotation angle. If we explicitly refer to the angle-axis parametrization of a rotation, we use the notation $g = g(\omega; \mathbf{n})$; accordingly, $\omega(g)$ and $\mathbf{n}(g)$ denote the angle and axis of rotation g, respectively.

The unit quaternion $q = \cos\frac{\omega}{2} + \mathbf{n}\sin\frac{\omega}{2}$, associated with the rotation $g = g(\omega; \mathbf{n})$, provides an embedding of the group SO(3) in the sphere $\mathbb{S}^3 \subset \mathbb{H}$ of unit quaternions.

Euler's theorem states that any two right-handed orthonormal coordinate systems can be related by a sequence of rotations (not more than three) about coordinate axes where two successive rotations must not be about the same axis. Then, any rotation g can be represented as a sequence of three successive rotations about conventionally specified coordinate axes by three corresponding "Euler" angles, where the rotation axes of two successive rotations must be orthonormal.

There exist 12 different choices of sets of axes of rotations (in terms of the coordinate axes of the initial coordinate system) to define corresponding Euler angles, and they are all in use somewhere.

Euler angles (α, β, γ) usually define a rotation g in terms of a sequence $g(\alpha, \beta, \gamma)$ of three successive rotations about conventionally fixed axes of the initial coordinate system, e.g., the first rotation by $\gamma \in [0, 2\pi)$ about the $\mathbf{z}$-axis, the second by $\beta \in [0, \pi]$ about the $\mathbf{y}$-axis, and the third by $\alpha \in [0, 2\pi)$ about the $\mathbf{z}$-axis of the initial coordinate system, such that

$$g(\alpha, \beta, \gamma) = g(\alpha; \mathbf{z})g(\beta; \mathbf{y})g(\gamma; \mathbf{z}). \tag{3}$$

In texture analysis, Bunge's definition of the Euler angles $(\varphi_1, \phi, \varphi_2)$ (Bunge 1982) of three successive rotations about conventionally fixed axes of rotations refers to the first rotation by $\varphi_1 \in [0, 2\pi)$ about the $\mathbf{z}$-axis, the second by $\phi \in [0, \pi]$ about the *rotated* $\mathbf{x}$-axis, i.e., about $\mathbf{x}' = g(\varphi; \mathbf{z})\mathbf{x}$, and the third by $\varphi_2 \in [0, 2\pi)$ about the *rotated* $\mathbf{z}$-axis, i.e., about $\mathbf{z}'' = g(\phi; \mathbf{x}')\mathbf{z}$, such that

$$g_{\text{Bunge}}(\varphi_1, \phi, \varphi_2) = g(\varphi_2; \mathbf{z}'')g(\phi; \mathbf{x}')g(\varphi_1; \mathbf{z}).$$

Roe's or Matthies' Euler angles (α, β, γ) (Matthies et al. 1987; Roe 1965) of three successive rotations about conventionally fixed axes of rotation replace Bunge's second rotation about $\mathbf{x}'$ by a rotation about the $\mathbf{y}'$-axis, i.e., they refer to the first rotation by $\alpha \in [0, 2\pi)$ about the $\mathbf{z}$-axis, the second by $\beta \in [0, \pi]$ about the *rotated* y-axis, i.e., about $\mathbf{y}' = g(\alpha; z)\mathbf{x}$, and the third by $\gamma \in [0, 2\pi)$ about the *rotated* $\mathbf{z}$-axis, i.e., about $\mathbf{z}'' = g(\beta; \mathbf{y}')\mathbf{z}$, such that

$$g_{\mathrm{RM}}(\alpha, \beta, \gamma) = g(\gamma, \mathbf{z}'')g(\beta, \mathbf{y}')g(\alpha; \mathbf{z}).$$

As can be shown by conjugation of rotations, the differently defined Euler angles are related by

$$g(\alpha, \beta, \gamma) = g_{\mathrm{RM}}(\alpha, \beta, \gamma).$$

Then, the Roe-Matthies notation has the simple advantage that (α, β) are the spherical coordinates of the crystallographic direction $\mathbf{c}$ with respect to $\mathcal{K}_S$.

3.2 Harmonics

Representation of rotations in terms of harmonics is a subject of representation theory as exposed in Gel'fand et al. (1963), Varshalovich et al. (1988), and Vilenkin and Klimyk (1991). Satisfying the representation property is the single most important characteristic of any useful system of functions for SO(3).

An important tool for the mathematical analysis of orientation probability and pole density functions are harmonic functions on the rotation group SO(3) and on the two-dimensional sphere $\mathbb{S}^2$, respectively. In fact, an orientation probability density function and its totally geodesic Radon transform share the same harmonic coefficients, which gives rise to a "harmonic approach" to the resolution of the inverse problem of texture analysis (Bunge 1965, 1969, 1982; Roe 1965). Furthermore, these harmonic coefficients are instrumental to compute the anisotropic macroscopic properties of a specimen, e.g., its thermal expansion, optical refraction index, electrical conductivity, or elastic properties, given the corresponding anisotropic properties of its single crystals.

Closely following the exposition in Hielscher (2007) and Hielscher and Schaeben (2008a), we render an explicit definition of harmonics as there are many slightly different ways to define them, e.g., with respect to normalization, which reveal their disastrous impact only in the course of writing and checking software code.

Harmonic analysis on the sphere is based on the Legendre polynomials $\mathcal{P}_\ell : [-1, 1] \to, \mathbb{R}, \ell \in \mathbb{N}_0$, where

$$\mathcal{P}_\ell(t) = \frac{1}{2^\ell \ell!} \frac{\mathrm{d}^\ell}{\mathrm{d}t^\ell}((t^2 - 1)^\ell),$$

and on the associated Legendre functions, $\mathcal{P}_\ell^k : [-1,1] \to \mathbb{R}$, $\ell \in \mathbb{N}_0$, $k = 0, \dots, \ell$,

$$\mathcal{P}_\ell^k(t) = \left(\frac{(\ell-k)!}{(\ell+k)!}\right)^{1/2} (1-t^2)^{k/2} \frac{\mathrm{d}^k}{\mathrm{d}t^k} \mathcal{P}_\ell(t).$$

In terms of the associated Legendre functions, we define the spherical harmonics $\mathcal{Y}_\ell^k(\mathbf{r})$,
$\ell \in \mathbb{N}_0$, $k = -\ell, \dots, \ell$, by

$$\mathcal{Y}_\ell^k(\mathbf{r}) = \sqrt{\frac{2\ell+1}{4\pi}} \mathcal{P}_\ell^{|k|}(\cos\ \theta) e^{ik\rho},$$

where $\theta, \rho \in \mathbb{R}$ are the polar coordinates $\rho \in [0, 2\pi)$, $\theta \in [0, \pi]$ of the vector

$$\mathbf{r} = (\cos\ \rho \sin\theta, \sin\rho \sin\theta, \cos\theta)^{\mathrm{T}} \in \mathbb{S}^2.$$

By this definition, the spherical harmonics are normed to

$$\int_{\mathbb{S}^2} \mathcal{Y}_\ell^k(\mathbf{r}) \overline{\mathcal{Y}_{\ell'}^{k'}}(\mathbf{r}) \mathrm{d}\mathbf{r} = \int_{\mathbb{S}^2} \mathcal{Y}_\ell^k(\theta,\rho) \overline{\mathcal{Y}_{\ell'}^{k'}(\theta,\rho)} \sin\theta\, \mathrm{d}\theta\, \mathrm{d}\rho = \delta_{\ell\ell'}\delta_{kk'}$$

and, hence, provide an orthonormal basis in $\mathrm{L}^2(\mathbb{S}^2)$.

In order to define harmonic functions on SO(3), we use the parameterization of a rotation $g \in \mathrm{SO}(3)$ in terms of Euler angles, Eq. (3). Now, we follow Nikiforov and Uvarov (1988) (see also Varshalovich et al. 1988, Kostelec and Rockmore 2003, Vollrath 2006) and define, for $\ell \in \mathbb{N}_0$, $k, k' = -\ell, \dots, \ell$, the generalized spherical harmonics or Wigner-D functions as

$$D_\ell^{kk'}(\alpha,\beta,\gamma) = e^{-ik\alpha} \mathrm{d}_\ell^{kk'}(\cos\beta) e^{-ik'\gamma},$$

where

$$\mathrm{d}_\ell^{kk'}(t) = S_{kk'} \frac{(-1)^{\ell-k'}}{2^\ell} \sqrt{\frac{(\ell+k')!}{(\ell-k')!(\ell+k)!(\ell-k)!}}$$
$$\times \sqrt{\frac{(1-t)^{k-k'}}{(1+t)^{k+k'}} \frac{\mathrm{d}^{\ell-k'}}{\mathrm{d}t^{\ell-k'}}} (1-t)^{\ell-k} (1+t)^{\ell+k}$$

and

$$S_{kk'} = \begin{cases} 1 & k, k' \geq 0, \\ (-1)^k & k' \geq 0,\ k < 0, \\ (-1)^{k'} & k \geq 0,\ k' < 0, \\ (-1)^{k+k'} & k, k' < 0. \end{cases}$$

The last term $s_{kk\prime}$ corrects for the normalization of the spherical harmonics, which are slightly different from those in Nikiforov and Uvarov (1988). The Wigner-D functions satisfy the representation property

$$D_\ell^{kk'}(gq) = \sum_{j=-\ell}^{\ell} D_\ell^{kj}(g) D_\ell^{jk'}(q), \tag{4}$$

and by virtue of the Peter-Weyl theorem (cf. Vilenkin 1968), they are orthogonal in $\mathrm{L}^2(\mathrm{SO}(3))$, i.e.,

$$\int_0^{2\pi}\int_0^{\pi}\int_0^{2\pi} D_\ell^{mn}(\alpha,\beta,\gamma)\overline{D_{\ell'}^{m'n'}(\alpha,\beta,\gamma)}\,\mathrm{d}\alpha\sin\beta\,\mathrm{d}\beta\,\mathrm{d}\gamma = \frac{8\pi^2}{2\ell+1}\delta_{\ell\ell'}\delta_{mm'}\delta_{nn'}.$$

Furthermore, they are related to the spherical harmonics by the representation property

$$\sum_{k'=-\ell}^{\ell} D_\ell^{kk'}(g)\mathcal{Y}_\ell^{k'}(\mathbf{h}) = \mathcal{Y}_\ell^{k}(g\mathbf{h}), \quad g \in \mathrm{SO}(3),\ \mathbf{h} \in \mathbb{S}^2.$$

Moreover, any (orientation density) function $f \in \mathrm{L}^2(\mathrm{SO}(3))$ has an associated harmonic or Fourier series expansion of the form

$$f \sim \sum_{\ell=0}^{\infty}\sum_{k,k'=-\ell}^{\ell} \frac{\left(\ell+\frac{1}{2}\right)^{\frac{1}{2}}}{2\pi}\hat{f}(\ell,k,k')D_\ell^{kk'},$$

with harmonic or Fourier coefficients

$$\hat{f}(\ell,k,k') = \frac{\left(\ell+\frac{1}{2}\right)^{\frac{1}{2}}}{2\pi}\int_{\mathrm{SO}(3)} f(g)\overline{D_\ell^{kk'}(g)}dg, \ell \in \mathbb{N}_0, k,k' = -\ell,\ldots,\ell.$$

Defined in this way, the classical Parseval identity

$$\left\|\hat{f}\right\|_{\ell_2} = \|f\|_{L^2}$$

is fulfilled; otherwise, e.g., for Bunge's C coefficients, it is not.

3.3 Kernels and Radially Symmetric Functions

In texture analysis, radially symmetric functions appear as unimodal bell-shaped model orientation density functions. Mathematically, they are defined as functions $\psi : \mathrm{SO}(3) \to \mathbb{R}$ or $\varphi : \mathbb{S}^2 \to \mathbb{R}$ that depend only on the distance to a center rotation $g_0 \in \mathrm{SO}(3)$ or a center direction $\mathbf{r}_0 \in \mathbb{S}^2$, respectively, i.e., we have

$$\psi(g) = \psi(g') \text{ and } \varphi(\mathbf{r}) = \varphi(\mathbf{r}')$$

for all rotations $g, g' \in \mathrm{SO}(3)$ with $\omega g g_0^{-1} = \omega g' g_0^{-1}$ and all directions $\mathbf{r}, \mathbf{r}' \in \mathbb{S}^2$ with $\eta(\mathbf{r}, \mathbf{r}_0) = \eta(\mathbf{r}', \mathbf{r}_0)$, where $\omega g g_0^{-1}$ denotes the rotational angle of the rotation g, g_0^{-1} and $\cos \eta(\mathbf{r}, \mathbf{r}_0) = \mathbf{r} \cdot \mathbf{r}_0$.

Radially symmetric functions, both on the rotation group as well as on the sphere, have characteristic Fourier series expansions. More precisely, there exist Chebyshev coefficients $\widehat{\psi(l)}$ and Legendre coefficients $\widehat{\varphi(l)}$, $l \in \mathbb{N}$, respectively,

$$\hat{\psi}(\ell, k, k') = \hat{\psi}(\ell) \overline{D_\ell^{kk'}(g_0)} \quad \text{and} \quad \hat{\varphi}(\ell, k) = \hat{\varphi}(l) \frac{4\pi}{2l+1} \overline{\mathcal{Y}_l^k(\mathbf{r}_0)},$$

such that

$$\psi(g) \sim \sum_{\ell=0}^{\infty} \hat{\psi}(l) \sum_{k,k'=-\ell}^{\ell} D_\ell^{kk'}(g) \overline{D_\ell^{kk'}(g_0)} \sim \sum_{\ell=0}^{\infty} \widehat{\psi(l)} \mathcal{U}_{2\ell}\left(\cos \frac{\omega(g g_0^{-1})}{2}\right) \tag{5}$$

and

$$\varphi(\mathbf{r}) \sim \sum_{l=0}^{\infty} \hat{\varphi}(l) \frac{4\pi}{2l+1} \sum_{k=-l}^{l} \mathcal{Y}_l^k(\mathbf{r}) \overline{\mathcal{Y}}_l^k(\mathbf{r_0}) \sim \sum_{l=0}^{\infty} \hat{\varphi}(l) \mathcal{P}_l(\mathbf{r} \cdot \mathbf{r}_0). \tag{6}$$

Here, $\mathcal{U}_l$, $l \in \mathbb{N}$, denote the Chebyshev polynomials of the second kind

$$\mathcal{U}_\ell(\cos \omega) = \frac{\sin(\ell+1)\omega}{\sin \omega}, \ell \in \mathbb{N}_0, \omega \in (0, \pi) \tag{7}$$

with $\mathcal{U}_\ell(1) = \ell + 1$ and $\mathcal{U}_\ell(-1) = (-1)^\ell \ell + 1$.

3.4 Crystallographic Symmetries

Considering crystallographic symmetries, Eq. (2), requires special provision. If the harmonics should be explicitly symmetrized such that they are properly defined on a left transversal $\mathbb{G} \subset \mathrm{SO}(3)$ only, then special attention should be paid to the preservation of the representation property, Eq. (4).

Here, a different approach is pursued in terms of radially symmetric functions ψ with known Chebyshev coefficients. Then, symmetrization is actually done by summation

$$\psi_{\mathrm{cs}}(\omega(g g_0^{-1})) = \frac{1}{\#\tilde{G}_{\mathrm{Laue}}} \sum_{q \in \tilde{G}_{\mathrm{Laue}}} \psi(\omega(g q g_0^{-1})), \quad g, g_0 \in \mathrm{SO}(3),\ q \in \tilde{G}_{\mathrm{Laue}}. \tag{8}$$

It is emphasized that ψ_{cs}, like ψ, is properly defined on SO(3), where numerical methods of fast summation are known (cf. Hielscher et al. 2010), which are, however, unknown for any subset of SO(3), such as $\mathbb{G}$. Moreover, the Fourier coefficients of ψ_{cs} can easily be computed from the Chebychev coefficients of ψ

$$\hat{\psi}_{\mathrm{cs}}(\ell,k,k') = \frac{\hat{\psi}(\ell)}{\#\tilde{G}_{\mathrm{Laue}}} \sum_{q\in\tilde{G}_{\mathrm{Laue}}} \sum_{j=-\ell}^{\ell} D_\ell^{kj}(q) D_\ell^{jk'}(g_0).$$

3.5 Geodesics, Hopf Fibres, and Clifford Tori

Then, some sets of rotations that are instrumental for texture analysis, as the (Hopf) fiber and the (Clifford) torus, are defined and characterized in terms of pairs (of sets) of unit vectors comprising an initial set of unit vectors and its image with respect to the elements of the set of rotation.

The distance between two rotations g_0, g is defined as the angle $\omega(g_0\ g^{-1})$ of the composition of the rotation g^{-1} followed by the rotation g_0.

The distance of a rotation g_0 from a set of rotations G is the infimum of all distances between the rotation and any element of the set of rotations, ie., $d(g_0, G) = \inf_{g\in G} \omega(g_0 g^{-1})$.

A one-dimensional submanifold of a Riemannian manifold is called geodesic if it is locally the shortest path between any two of its points. Any geodesic $G \in \mathrm{SO}(3)$ can be parametrized by two unit vectors and is defined as fiber

$$G = G(\mathbf{h},\mathbf{r}) = \{g \in \mathrm{SO}(3) | g\mathbf{h} = \mathbf{r}\}, \tag{9}$$

where the vectors $\mathbf{h},\mathbf{r} \in \mathbb{S}^2$ are well defined up to the symmetry $G(\mathbf{h},\mathbf{r}) = G(-\mathbf{h},-\mathbf{r})$ (Hielscher 2007; Meister and Schaeben 2004). The geodesics induce a double fibration of SO(3) and may be referred to as Hopf fibers (Vajk 1995; Kreminski 1997; Chisholm, The sphere in three dimensions and higher: generalizations and special cases. Personal Communication, 2000).

In terms of unit quaternions $q_1, q_2 \in \mathbb{S}^3$ associated with rotations $g_1, g_2 \in \mathrm{SO}(3)$, their geodesic $G(\mathbf{h},\mathbf{r})$ obviously corresponds to the great circle $C(q_1, q_2) \subset \mathbb{S}^3$ with pure quaternions

$$h = q_1^* q_2, \quad r = q_2 q_1^*.$$

Given a pair of unit vectors $(\mathbf{h},\mathbf{r}) \in \mathbb{S}^2 \times \mathbb{S}^2$ with $\mathbf{h} \times \mathbf{r} \neq 0$, the geodesic $G(\mathbf{h},\mathbf{r})$ is associated with the great circle $C(q_1,\ q_2)$ of unit quaternions spanned by orthonormal quaternions

$$q_1 = \frac{1}{\|1 - rh\|}(1 - rh) = \cos\frac{\eta}{2} + \frac{\mathbf{h}\times\mathbf{r}}{\|\mathbf{h}\times\mathbf{r}\|}\sin\frac{\eta}{2}, \tag{10}$$

$$q_2 = \frac{1}{\|h + r\|}(h + r) = 0 + \frac{\mathbf{h} + \mathbf{r}}{\|\mathbf{h} \times \mathbf{r}\|}, \tag{11}$$

where $\eta = \eta(\mathbf{h}, \mathbf{r})$ denotes the angle between $\mathbf{h}$ and $\mathbf{r}$, i.e., $\cos \eta = \mathbf{h} \cdot \mathbf{r}$.

Since r and h are pure unit quaternions, we get

$$r(1 - rh) = (1 - rh)h = h + r,$$

and obviously, $||1 - rh|| = ||h + r||$. Then, with Eqs. (10) and (11),

$$rq_1 = q_1 h = q_2, \tag{12}$$

i.e., rq_1 and $q_1 h$ also represent rotations mapping $\mathbf{h}$ onto $\mathbf{r}$. Moreover, it should be noted that Eq. (12) implies

$$q_2^* r q_1 = 1, \quad q_1 h q_2^* = 1,$$

which may be interpreted as a remarkable "factorization" of 1 (Meister and Schaeben 2004).

The distance of an arbitrary rotation g_0 from the fiber $G(\mathbf{h}, \mathbf{r})$ or, referring to the quaternionic embedding, the distance of $q_0 \in \mathbb{S}^3$ from the circle $C(q_1, q_2)$ is given by

$$\mathrm{d}(g, G(\mathbf{h}, \mathbf{r})) = \frac{1}{2}\arccos(g\mathbf{h} \cdot \mathbf{r}), \quad \mathrm{d}(q, C(q_1, q_2)) = \frac{1}{2}\arccos(q\mathbf{h}q^* \cdot \mathbf{r})$$

(Kunze 1991; Meister and Schaeben 2004).

Let q_1, q_2, q_3, and q_4 denote four mutually orthonormal quaternions. Then, the Clifford torus $T(q_1, q_2, q_3, q_4; \Theta) \subset \mathbb{S}^3$ (Chisholm, The sphere in three dimensions and higher: generalizations and special cases. Personal Communication, 2000), defined as the set of quaternions

$$\begin{aligned} q(s, t; \Theta) = {} & (q_1 \cos s + q_2 \sin s) \cos \Theta + (q_3 \cos t + q_4 \sin t) \sin \Theta, \\ & s, t \in [0, 2\pi), \Theta \in [0, \pi/2], \end{aligned} \tag{13}$$

consists of all great circles with distance $\cos\Theta$ from the geodesic $C(q_1, q_2)G(\mathbf{h}, \mathbf{r})$, i.e., $T(q_1, q_2, q_3, q_4; \Theta) = T(G(\mathbf{h}, \mathbf{r}); \Theta)$. It is associated with all rotations mapping $\mathbf{h}$ on the small circle $c(\mathbf{r}, 2\Theta) \subset \mathbb{S}^2$ and mapping the small circle $c(\mathbf{h}, 2\Theta) \subset \mathbb{S}^2$ on $\mathbf{r}$, respectively (Meister and Schaeben 2004). It should be noted that Eq. (13) can be suitably factorized (Meister and Schaeben 2004).

4 Totally Geodesic Radon Transforms

For any function f integrable on each fiber $G(\mathbf{h}, \mathbf{r})$, the totally geodesic Radon transform $\mathcal{R}f$ assigns the mean values along any fiber to f, i.e.,

$$\mathcal{R}f(\mathbf{h}, \mathbf{r}) = \frac{1}{2\pi} \int_{G(\mathbf{h},\mathbf{r})} f(g)\mathrm{d}g. \tag{14}$$

It provides the density of the probability that the random crystal direction $g\mathbf{h}$ coincides with the specimen direction $\mathbf{r}$, given the random rotation g. Accounting for Friedel's law (Friedel 1913) that diffraction cannot distinguish between the positive and negative normal vector of a lattice plane, it is

$$P(\mathbf{h}, \mathbf{r}) = \frac{1}{2} \left(\mathcal{R}f(\mathbf{h}, \mathbf{r}) + \mathcal{R}f(-\mathbf{h}, \mathbf{r})\right) = \chi f(\mathbf{h}, \mathbf{r}), \tag{15}$$

where $\mathcal{X}f(\mathbf{h}, \mathbf{r})$ is also referred to as the basic *crystallographic* X-ray transform (Nikolayev and Schaeben 1999; Schaeben 2001). While the totally geodesic Radon transform possesses a unique inverse (Helgason 1994, 1999), the crystallographic X-ray transform does not. The kernels of the latter are the harmonics of odd order (Matthies 1979), see below.

Further following Helgason (1994, 1999), the generalized totally geodesic Radon transform and the respective dual are well defined. The generalized totally geodesic Radon transform of a real function $f : \mathrm{SO}(3) \to \mathbb{R}$ is defined as

$$\mathcal{R}^{(\rho)} f(\mathbf{h}, \mathbf{r}) = \frac{1}{4\pi^2 \sin 2\rho} \int_{\mathrm{d}(g,G(\mathbf{h},\mathbf{r}))=\rho} f(g)\, \mathrm{d}g.$$

It associates with f its mean values over the torus $T(G(\mathbf{h}, \mathbf{r});\rho)$ with core $G(\mathbf{h}, \mathbf{r})$ and radius ρ (Eq. 13). For $\rho = 0$, the generalized totally geodesic Radon transform converges toward the totally geodesic Radon transform.

Then, we may state the following theorem: The generalized totally geodesic Radon transform is equal to the spherically translated totally geodesic Radon transform, and it can be identified with the angle density function

$$\begin{aligned} \left(\mathcal{T}^{(\rho)}[\mathcal{R}f]\right)(\mathbf{h}, \mathbf{r}) &= \frac{1}{2\pi \sin\rho} \int_{c(\mathbf{h};\rho)} \mathcal{R}f(\mathbf{h}', \mathbf{r})\mathrm{d}\mathbf{h}' \\ &= \frac{1}{2\pi \sin\rho} \int_{c(\mathbf{r};\rho)} \mathcal{R}f(\mathbf{h}, \mathbf{r}')\mathrm{d}\mathbf{r}' \end{aligned} \tag{16}$$

$$= \frac{1}{4\pi^2 \sin\rho} \int_{c(\mathbf{r};\rho)} \int_{G(\mathbf{h},\mathbf{r}')} f(g)\mathrm{d}g\, d\mathbf{r}' \tag{17}$$

$$= \frac{1}{4\pi^2 \sin\rho} \int_{T(G(\mathbf{h},\mathbf{r});\frac{\rho}{2})} f(g)\mathrm{d}g \tag{18}$$

$$\begin{aligned} &= \frac{1}{4\pi^2 \sin\rho} \int_{\mathrm{d}(g,G(\mathbf{h},\mathbf{r}))=\frac{\rho}{2}} f(q)\mathrm{d}q \\ &= \mathcal{R}^{(\rho/2)} f(C_{\mathbf{h},\mathbf{r}}). \end{aligned} \tag{19}$$

Thus,

$$\left(\mathcal{T}^{(\rho)}[\mathcal{R}f]\right)(\mathbf{h},\mathbf{r}) = \mathcal{R}^{(\rho/2)} f(\mathbf{h},\mathbf{r}) = \mathcal{A}f(\mathbf{h},\mathbf{r};\rho) \tag{20}$$

(Bernstein et al. 2009). The angle density function $\mathcal{A}f(\mathbf{h},\mathbf{r};\rho)$ has been introduced into texture analysis by Bunge, e.g., Bunge (1969, p. 44, 1982, p. 74) (with a false normalization). According to its definition, it is the mean value of the pole density function over a small circle $c(\mathbf{h};\rho)$ centered at $\mathbf{r}$, a construct known as spherical translation $(\mathcal{T}^{(\rho)}[\mathcal{R}f])(\mathbf{h},\mathbf{r})$ in spherical approximation. Thus, it is the density that the crystallographic direction $\mathbf{h}$ encloses the angle $\rho, 0 \le \rho \le \pi$ with the specimen direction $\mathbf{r}$, given the orientation probability density function f. Equation (16), i.e., the commutation of the order of integration, has been observed without reference to Radon transforms or Ásgeirsson means and stated without proof (cf. Bunge 1969, p. 47; 1982, p. 76), not to mention purely geometric arguments.

Nevertheless, its central role for the inverse Radon transform was recognized in Muller et al. (1981) by "rewriting" Matthies' inversion formula (Matthies 1979).

It should be noted that

$$\mathcal{A}f(\mathbf{h},\mathbf{r};0) = \mathcal{R}f(\mathbf{h},\mathbf{r}), \quad \mathcal{A}f(\mathbf{h},\mathbf{r};\pi) = \mathcal{R}f(\mathbf{h},-\mathbf{r}).$$

The key to the analytical inverse of the totally geodesic Radon transform is provided by the dual Radon transforms (Helgason 1999).

4.1 Properties of the Spherical Radon Transform

In this section, we compile the properties of the totally geodesic Radon transform which are fundamental to understand the mathematics of texture analysis.

Antipodal Symmetry

On its domain of definition, the one-dimensional Radon transform, $\mathcal{R}f$ of any function $f : \mathrm{SO}(3) \to \mathbb{R}$ has the symmetry property $\mathcal{R}f(-\mathbf{h},\mathbf{r}) = \mathcal{R}f(\mathbf{h},-\mathbf{r})$. The crystallographic X-ray transform satisfies the additional symmetry property $\mathcal{X}f(\mathbf{h},\mathbf{r}) = \mathcal{X}f(-\mathbf{h},\mathbf{r}) = \mathcal{X}f(\mathbf{h},-\mathbf{r})$. Thus, pole figures correspond to the crystallographic transform, which is even in both arguments.

Effect of Crystallographic Symmetry

If, for a symmetry group $\tilde{G}_{\text{Laue}} \subset \text{SO}(3)$, a function f satisfies $f(gq) = f(g)$ for all $g \in \text{SO}(3)$, $q \in \tilde{G}_{\text{Laue}}$, its corresponding Radon transform $\mathcal{R}f$ satisfies

$$\mathcal{R}f(q\mathbf{h}, \mathbf{r}) = \mathcal{R}[f(\circ q^{-1})](\mathbf{h}, \mathbf{r}) = \mathcal{R}[f(\circ)](\mathbf{h}, \mathbf{r}) = \mathcal{R}f(\mathbf{h}, \mathbf{r})$$

for all $q \in \tilde{G}_{\text{Laue}}$.

Radial Symmetry

If the orientation probability density function is radially symmetrical with respect to $g_0 \in \text{SO}(3)$, i.e., if it depends on the angle of rotation only, the Radon transform is radially symmetric too. More specifically and formally, let f be of the form

$$f(g) = f(\omega(gg_0^{-1})), g_0 \in \text{SO}(3).$$

Then, the Radon transform $\mathcal{R}f(\mathbf{h}, \mathbf{r})$ defined on $\mathbb{S}^2 \times \mathbb{S}^2$ is radially symmetrical with respect to $\mathbf{r}_0 = g_0\mathbf{h}$, i.e., $\mathcal{R}f(\mathbf{h}, \circ)$ is radially symmetric with respect to $g_0\mathbf{h}$, and $\mathcal{R}f(\circ, \mathbf{r})$ is radially symmetric with respect to $g_0^{-1}\mathbf{r}$. Thus, the Radon transform reduces to a function $\mathcal{R}f(g_0\mathbf{h} \cdot \mathbf{r})$ defined on [-1, 1] and may be thought of as depending on the angle $\eta = \arccos(g_0\mathbf{h} \cdot \mathbf{r}) \in [0, \pi]$.

In particular, the Chebyshev coefficients $\widehat{\psi(l)}$ of a radially symmetric orientation density function ψ coincide with the Legendre coefficients of its Radon transform $\mathcal{R}\psi(\mathbf{h}, \cdot)$, i.e.,

$$\mathcal{R}\psi(\mathbf{h}, \mathbf{r}) \sim \sum_{l=0}^{\infty} \widehat{\psi(l)} \mathcal{P}_l(g_0\mathbf{h} \cdot \mathbf{r}), \quad \mathbf{h}, \mathbf{r} \in \mathbb{S}^2. \tag{21}$$

It should be noted that the radial symmetry of f with respect to $g_0 \in \text{SO}(3)$ is necessary and sufficient for the radial symmetry of the transform $\mathcal{R}f(\mathbf{h}, \mathbf{r})$ with respect to $\mathbf{r}_0 = g_0\mathbf{h}$ (Schaeben 1997).

If the orientation probability density function is a fiber symmetric function, i.e., if f is of the form

$$f(g) = f(g\mathbf{h}_0 \cdot \mathbf{r}_0), (\mathbf{h}_0, \mathbf{r}_0) \in \mathbb{S}^2 \times \mathbb{S}^2,$$

then $\mathcal{R}f(\mathbf{h}, \circ)$ is radially symmetric with respect to $\mathbf{r}_0$, and $\mathcal{R}f(\circ, \mathbf{r})$ is radially symmetric with respect to $\mathbf{h}_0$ (Hielscher 2007).

Special cases of the even Bingham quaternion distribution on $\mathcal{S}^3$ or, eqivalently, of the Fisher von Mises matrix distribution on SO(3) comprise a bimodal "bipolar," a circular "fiber," and an often overlooked spherical "surface" distribution (Kunze and Schaeben 2004).

Darboux Differential Equation

The Radon transform satisfies a Darboux-type differential equation

$$(\Delta_{\mathbf{h}} - \Delta_{\mathbf{r}})\mathcal{R}f(\mathbf{h},\mathbf{r}) = 0, \tag{22}$$

where Δ_h denotes the Laplace-Beltrami operator applied with respect to $\mathbf{h} \in \mathbb{S}^2$ (Savyolova 1994). Its general solution has been derived in terms of harmonics and in terms of characteristics, respectively (Nikolayev and Schaeben 1999).

Fourier Slice Theorem

The following well-known theorem, dating back to the origin of texture analysis, characterizes the relationship between the Fourier expansion of an orientation density function and its corresponding pole density function. Let $f \in \mathrm{L}^2(\mathrm{SO}(3))$ be an orientation density function with Fourier expansion

$$f \sim \sum_{\ell=0}^{\infty} \sum_{k,k'=-\ell}^{\ell} \frac{(\ell+\frac{1}{2})^{\frac{1}{2}}}{2\pi} \hat{f}(\ell,k,k') D_\ell^{kk'}.$$

Then, the corresponding pole density function $P \in \mathrm{L}^2(\mathbb{S}^2 \times \mathbb{S}^2)$, $P(\mathbf{h},\mathbf{r}) = \frac{1}{2}(\mathcal{R}f(\mathbf{h},\mathbf{r}) + \mathcal{R}f(-\mathbf{h},\mathbf{r}))$ possesses the associated Fourier expansion

$$P(\mathbf{h},\mathbf{r}) = \mathcal{X}f(\mathbf{h},\mathbf{r}) \sim \sum_{\ell \in 2\mathbb{N}_0} \sum_{k,k'=-\ell}^{\ell} \frac{1}{(\ell+\frac{1}{2})^{\frac{1}{2}}} \hat{f}(\ell,k,k') \mathcal{Y}_\ell^{k'}(\mathbf{h}) \overline{\mathcal{Y}_\ell^{k}(\mathbf{r})}. \tag{23}$$

The theorem states that the Radon transform preserves the order of harmonics

$$\mathcal{R}D_\ell^{kk'}(\mathbf{h},\mathbf{r}) = \frac{2\pi}{\ell+\frac{1}{2}} \mathcal{Y}_\ell^{k'}(\mathbf{h}) \overline{\mathcal{Y}_\ell^{k}(\mathbf{r})}, \tag{24}$$

and, moreover, that a function $f : \mathrm{SO}(3) \to \mathbb{R}$ and its Radon transform $\mathcal{R}f : \mathbb{S}^2 \times \mathbb{S}^2 \to \mathbb{R}$ have the same harmonic coefficients up to scaling. In particular, it states that the crystallographic X-ray transform, Eq. (15), of any odd-order harmonic vanishes, i.e.,

$$\mathcal{X}D_\ell^{kk'} \equiv 0 \text{ for all odd } \ell. \tag{25}$$

Thus, the crystallographic X-ray transform has a nonempty kernel comprising the harmonics of odd order.

For a modern account of the Fourier slice theorem, the reader is referred to Hielscher et al. (2008).

Range

The range of an operator $A : \mathcal{D} \to \mathcal{Y}$ is defined as the subspace of all functions $P \in \mathcal{Y}$ such that there is a function $f \in \mathcal{D}$ with $Af = P$. In the case of the Radon transform, a characterization of the range can be derived directly from Eq. (24).

More specifically, the image of $L^2(SO(3))$ with respect to the Radon transform can be derived by comparison of Eq. (23) with

$$u(\mathbf{h},\mathbf{r}) \sim \sum_{\ell\in 2\mathbb{N}_0} \sum_{k,k'=-\ell}^{\ell} \hat{u}(\ell,k,k')\mathcal{Y}_\ell^{k'}(\mathbf{h})\overline{\mathcal{Y}_\ell^{k}(\mathbf{r})}$$

resulting in

$$\begin{aligned}\mathcal{R}L^2(SO(3)) &= \{u(\mathbf{h},\mathbf{r}) = \textstyle\sum \frac{1}{(\ell+\frac{1}{2})^{\frac{1}{2}}} \hat{f}(\ell,k,k')Y_\ell^m(\mathbf{h})Y_\ell^n(\mathbf{r}) | \sum (\hat{f}(\ell,k,k'))^2 < \infty\} \\ &= \{u(\mathbf{h},\mathbf{r}) = \textstyle\sum \hat{u}(\ell,k,k')Y_\ell^m(\mathbf{h})Y_\ell^n(\mathbf{r}) | \sum (\ell+\frac{1}{2})(\hat{u}(\ell,k,k'))^2 < \infty\}\end{aligned}$$

(Hielscher 2007), indicating the smoothing effect of the Radon transform as already to be recognized by the Darboux differential equation. For an equivalent characterization of the range of the Radon transform directly by means of the differential equation, we refer to Nikolayev and Schaeben (1999). In particular, the characteristics of the differential equation lead to the following representation of a Radon transformed function as a superposition of radially symmetric functions

$$\mathcal{R}f(\mathbf{h},\mathbf{r}) = \sum\nolimits_\ell \sum\nolimits_k u_\ell(\mathbf{h}\cdot g_k^{-1}\mathbf{r}), \tag{26}$$

where $g_k \in SO(3)$ are arbitrary orientations and $u_\ell \in C^2(\mathbb{R}^1)$ are some appropriately chosen, real, twice differentiable functions (Nikolayev and Schaeben 1999). The functions u_ℓ are radially symmetrical with respect to $g_k^{-1}\mathbf{r}$, or $g_k\mathbf{h}$, $k = 1,\ldots,K$, respectively.

Inverse Radon Transform

In texture analysis, i.e., in material science and engineering, the best-known inversion formula dates back right to the beginning of "quantitative" texture analysis (Bunge 1965; Roe 1965). The formula may be rewritten in a rather abstract way as

$$f = \mathcal{F}_{SO(3)}^{-1}\mathcal{S}\mathcal{F}_{\mathbb{S}^2\times\mathbb{S}^2}\mathcal{R}f, \tag{27}$$

where $\mathcal{S}$ denotes a scaling matrix, with entries $\sqrt{2\ell+1}$ indicating the ill-posedness of the inverse problem. It applies the Fourier slice theorem. In the context of texture analysis and experimentally accessible "pole figures," the former statement is true only for even-order coefficients because of Eq. (25).

There are more inversion formulas (cf. Helgason 1984, 1999), involving the Laplacian operator for $\mathbb{S}^2$ and SO(3). They are equivalent to the formula by Matthies (1979), rewritten in terms of the angle probability density function (Muller et al. 1981). For a comprehensive exposition, the reader is referred to Bernstein and Schaeben (2005).

Loss of Non-negativity

Obviously, if $f \geq 0$, then $\mathcal{R}f \geq 0$. However, the non-negativity of $\mathcal{R}f$ does not imply the non-negativity of f. This loss of non-negativity causes essential problems of the harmonic method for inversion of the crystallographic X-ray transform as it is unknown how the non-negativity constraint $f \geq 0$ could be turned into a constructive element of the harmonic approach (Watson 1969). Moreover, once an approximation $f*$ is found in terms of its Fourier coefficients such that its X-ray transform $\mathcal{X}f*$ is non-negative, the non-negativity of $f*$ is not guaranteed. Even worse, if $f*$ happens to be not non-negative, then it is not at all clear if an odd "complement" exists to correct $f*$ such that the resulting new approximation is non-negative.

Finite Support Property

If f vanishes outside the spherical cap $B(g_0;\varepsilon) = \{g \in \mathrm{SO}(3) \,|\omega(g_0, g) \leq \varepsilon\}$, then its Radon transform $\mathcal{R}f$ vanishes outside the corresponding spherical cap $\mathcal{R}B(g_0,\epsilon) = \{(\mathbf{h},\mathbf{r}) \in \mathbb{S}^2 \times \mathbb{S}^2 | \boldsymbol{\omega}(\mathbf{g_0 h},\mathbf{r}) < \epsilon\}$; here, $\mathcal{R}B(g_0,\varepsilon)$ denotes the set of all fibers intersecting $B(\mathbf{g}_0,\varepsilon)$ (Hielscher 2007).

Localization

The inversion of the Radon transform would be local if, for any open subset $U \subset SO(3)$, the condition $\mathcal{R}f(\mathbf{h},\mathbf{r}) = 0$ for all $(\mathbf{h},\mathbf{r}) \in \mathbb{S}^2 \times \mathbb{S}^2$ with $G(\mathbf{h},\mathbf{r}) \cap U \neq \emptyset$ implies $f|_U = 0$ for any function $f \in C(\mathrm{SO}(3))$. Unfortunately, the inversion of the Radon transform on SO(3) is not local. An explicit counterexample is given in Hielscher (2007). Thus, in order to recover the value of a function $f \in C(\mathrm{SO}(3))$ for an individual $g \in \mathrm{SO}(3)$, the integrals along all one-dimensional geodesics of SO(3) have to be known. The missing localization of the inverse Radon transform may be seen as a strong motivation to apply the corresponding multiscale representations (Hielscher and Schaeben 2008b) of both, the orientation probability density function and its totally geodesic Radon transform as "second-best" approach to recover an orientation probability density function in a small subset of SO(3) only. With radially symmetric kernels, multiscale representation is mimicked by arbitrarily irregular grids and a "zero-domain" approach (Hielscher 2007; Hielscher and Schaeben 2008a; Schaeben 2007).

5 Texture Analysis with Integral Orientation Measurements: Texture Goniometry Pole Intensity Data

A detailed introduction to diffraction at a single crystal can be found in Forsyth (1988) and Randle and Engler (2000). For diffraction of polycrystalline materials, we refer also to Randle and Engler (2000). Here, we only give the basic facts necessary for a simple, yet effective, mathematical model.

An initially deterministic normalized model for the diffraction intensity $I_{\mathrm{norm}}(\lambda,\theta,\mathbf{r})$ originating from a polycrystalline specimen for a wavelength λ, a Bragg angle θ, and a specimen direction $\mathbf{r}$, controlled by the texture goniometer, is provided by

$$I_{\text{norm}}(\lambda, \theta, \mathbf{r}) = \left(\sum_{\mathbf{h} \in H(\lambda,\theta)} \rho(\mathbf{h}) \right)^{-1} \sum_{\mathbf{h} \in H(\lambda,\theta)} \rho(\mathbf{h}) \mathcal{R} f(\mathbf{h}, \mathbf{r}),$$

where $H(\lambda, \theta) \subset \mathbb{S}^2$ denotes the set of vectors normal to the lattice planes responsible for diffraction, given the specific combination of a wavelength λ and a Bragg angle θ, and where $\rho(\mathbf{h})$ denotes the structure coefficients of the diffracting lattice planes $\mathbf{h} \in H(\lambda, \theta)$ (Randle and Engler 2000). The set $H(\lambda, \theta)$ is symmetrical with respect to the restricted Laue group $\tilde{G}_{\text{Laue}} \subset \text{SO}(3)$, i.e., with $\mathbf{h} \in H(\lambda, \theta)$, we have $q\mathbf{h} \in H(\lambda, \theta)$ for any symmetry element $q \in \tilde{G}_{\text{Laue}}$.

Additionally, Friedel's law (Friedel 1913) implies $-\mathbf{h} \in H(\lambda, \theta)$ for any $\mathbf{h} \in H(\lambda, \theta)$.

In practice, normalized diffraction intensities are not accessible, but only absolute particle counts are measured, which are affected by background radiation $I^b(\lambda, \theta, \mathbf{r})$ and measurement errors and differ from the normalized intensities by an unknown normalization factor $\nu(\lambda, \theta)$. Then, we have, for the absolute intensity,

$$I_{\text{abs}}(\lambda, \theta, \mathbf{r}) = \nu(\lambda, \theta) \sum_{\mathbf{h} \in H(\lambda,\theta)} \rho(\mathbf{h}) \mathcal{R} f(\mathbf{h}, \mathbf{r}) + I^b(\lambda, \theta, \mathbf{r}).$$

Since particle counts can generally be modeled with a Poisson distribution with its mean value set to the absolute intensity (Randle and Engler 2000), we obtain, for an individual diffraction measurement, the statistical model

$$I(\lambda, \theta, \mathbf{r}) \sim \text{Pois} \left(\nu(\lambda, \theta) \sum_{\mathbf{h} \in H(\lambda,\theta)} \rho(\mathbf{h}) \mathcal{R} f(\mathbf{h}, \mathbf{r}) + I^b(\lambda, \theta, \mathbf{r}) \right) \tag{28}$$

characterizing it as a one-element random sample of a parameterized Poisson process. This model implies that the standard deviation of diffraction counts is approximately

$$\sigma_{I(\lambda,\theta,\mathbf{r})} = \sqrt{I_{\text{abs}}(\lambda, \theta, \mathbf{r})} \approx \sqrt{I(\lambda, \theta, \mathbf{r})}, \tag{29}$$

(cf. Wenk 1985, p. 37).

It should be noted that Eq. (28) is only a very simple model for experimental diffraction counts. First of all, Bragg's law itself is only a rough simplification of much more sophisticated models explaining diffraction, e.g., Cowley (1995). Second, the diffraction counts commonly used for texture determination are obtained by processing a spectrum of diffraction counts for varying Bragg angles θ or wavelengths λ (Hammond 1997; Randle and Engler 2000).

The inverse problem, to determine f from Eq. (28), can be interpreted as a classical parameter estimation problem, with the orientation density function f and the normalization coefficient ν as the unknown parameters, given the diffraction pole density functions.

In a diffraction experiment with a texture goniometer, diffraction counts with respect to several diffraction parameters and several specimen directions are measured. We enumerate the sequence of diffraction parameters $(\lambda, \theta)_i$ and the corresponding sequence of lattice planes $H_i = H((\lambda, \theta)_i) \subset \mathbb{S}^2$ by the index $i = 1, \ldots, N$. If superposition of pole figures does not occur, the sequence $H_i, i = 1, \ldots, N$, corresponds simply to the sequence of measured lattice planes. For each pair $(\lambda, \theta)_i, i = 1, \ldots, N$, of a wavelength and a Bragg angle, we enumerate the specimen directions $\mathbf{r}_{ij_i} \in \mathbb{S}^2$, with respect to which diffraction intensities are measured by the indices $j_i = 1, \ldots, N_i$. Correspondingly, we abbreviate the diffraction counts by $I_{ij_i} = I(\lambda_i, \theta_i, \mathbf{r}_{ij_i})$ and the background intensities by $I^b_{ij_i} = I^b(\lambda_i, \theta_i, \mathbf{r}_{ij_i})$. The indexing $ij_i, i = 1, \ldots, N, j_i = 1, \ldots, N_i$, applies to arbitrarily scattered specimen directions of each pole density function individually.

Then, we may consider the least squares estimator

$$(f_{\mathrm{LS}}, \nu_{\mathrm{LS}}) = \operatorname{argmin} \sum_{i=1}^{N} \sum_{j_i=1}^{N_i} \frac{\left(\nu_i \mathcal{R} f(H_i, \mathbf{r}_{ij_i}) + I^b_{ij_i} - I_{ij_i}\right)^2}{I_{ij_i}}, \tag{30}$$

subject to the constraints

$$\nu \geq 0, f \geq 0 \quad \text{and} \quad \int_{\mathrm{SO}(3)} f(g) \mathrm{d}g = 8\pi^2.$$

This estimator may be regularized by adding a Sobolev norm $\lambda ||f||_{\mathcal{H}(\mathrm{SO}(3))}$ of the orientation density function f as a penalty term. This penalty term can be interpreted as the prior information on the unknown orientation density function to be smooth.

Due to the unknown normalization coefficients $\boldsymbol{\nu} = (\nu_1, \ldots, \nu_N)^T$, the functional Eq. (30) is neither linear nor convex, and hence, the minimization problem may have several solutions (Hielscher 2007). Another problem inherent in the minimization problem (Eq. 30) is that common algorithms result in solutions tending to be unstable and largely dependent on the initial guess of the unknown parameters f and $\boldsymbol{\nu}$ (Hielscher 2007). A more robust estimator is obtained when the unknown normalization coefficients, $\nu_i, i = 1, \ldots, N$, in the LS-estimator are replaced by their quadrature rule estimators

$$\tilde{\nu}_i(f) = \frac{\sum_{j_i=1}^{N_i} I_{ij_i} - I^b_{ij_i}}{\sum_{j_i=1}^{N_i} \mathcal{R} f(H_i, \mathbf{r}_{ij_i})}.$$

We call the resulting estimator

$$f_{\mathrm{MLS}} = \operatorname{argmin} \sum_{i=1}^{N} \sum_{j_i=1}^{N_i} \frac{\left(\tilde{\nu}_i(f)\mathcal{R}f(H_i, \mathbf{r}_{ij_i}) + I^b_{ij_i} - I_{ij_i}\right)^2}{I_{ij_i}} + \lambda ||f||^2_{\mathcal{H}(\mathrm{SO}(3))} \tag{31}$$

a modified least squares estimator.

The representation of the orientation density function estimation problem as a least squares problem, which includes the unknown normalization coefficients as unknown variables, dates back to Van Houtte (1980); Van Houtte (1984). Weighting the least squares functionals Eqs. (30) and (32) with the inverse expected variance I_{ij}^{-1} of the measurement error Eq. (29), we ensure the homoscedasticity of the underlying regression problem. The regularization term $\lambda ||f||_{\mathcal{H}(\mathrm{SO}(3))}$ was first suggested in Bernier et al. (2006) and Van den Boogaart et al. (2007) and can be interpreted as a model assumption on the true orientation density function that biases the estimator toward smoother orientation density functions.

In a final discretization step, we apply the modeling assumption that the unknown orientation probability density function f can be approximated by a non-negative linear combination

$$f(g) = \sum\nolimits_{m=1}^{M} c_m \ \psi \ \mathrm{cs}(g g_m^{-1}) = \sum_{m=1}^{M} \sum_{q \in \tilde{G}_{\mathrm{Laue}}} c_m \psi(\omega(q g g_m^{-1}))$$

of non-negative symmetrized kernel functions ψ_{cs}, Eq. (8), centered at nodes $g_1, \ldots, g_M \in \mathrm{SO}(3)$, with non-negative unknown coefficients $c_m \geq 0, m = 1, \ldots, M$. Since the Radon transform is linear, we get

$$\mathcal{R}f(\mathbf{h}, \mathbf{r}) = \frac{1}{\#\tilde{G}_{\mathrm{Laue}}} \sum_{m=1}^{M} \sum_{q \in \tilde{G}_{\mathrm{Laue}}} c_m \mathcal{R}\psi(q g_m \mathbf{h} \cdot \mathbf{r}) = \frac{1}{\#\tilde{G}_{\mathrm{Laue}}} \sum_{m=1}^{M} \sum_{q \in \tilde{G}_{\mathrm{Laue}}} c_m \varphi(q g_m \mathbf{h} \cdot \mathbf{r})$$

to yield

$$\mathbf{c}_{\mathrm{MLS}} = \operatorname{argmin} \sum_{i=1}^{N} \sum_{j_i=1}^{N_i} \frac{\left(\tilde{\nu}_i(f) \frac{1}{\#\tilde{G}_{\mathrm{Laue}}} \sum_{m=1}^{M} \sum_{q \in \tilde{G}_{\mathrm{Laue}}} c_m \varphi(q g_m H_i \cdot \mathbf{r}_{ij_i}) + I^b_{ij_i} - I_{ij_i}\right)^2}{I_{ij_i}} + \lambda ||f||^2_{\mathcal{H}(\mathrm{SO}(3))}. \tag{32}$$

An example of a well-localized, non-negative, radially symmetric function on SO(3) is the *de la Vallée Poussin* kernel (Hielscher 2007; Schaeben 1997, 1999). It is given for any $\kappa \in \mathbb{N}$ by

$$\psi(g) = \frac{B\left(\frac{3}{2}, \frac{1}{2}\right)}{B\left(\frac{3}{2}, \kappa + \frac{1}{2}\right)} \cos^{2\kappa} \frac{\omega(g)}{2}.$$

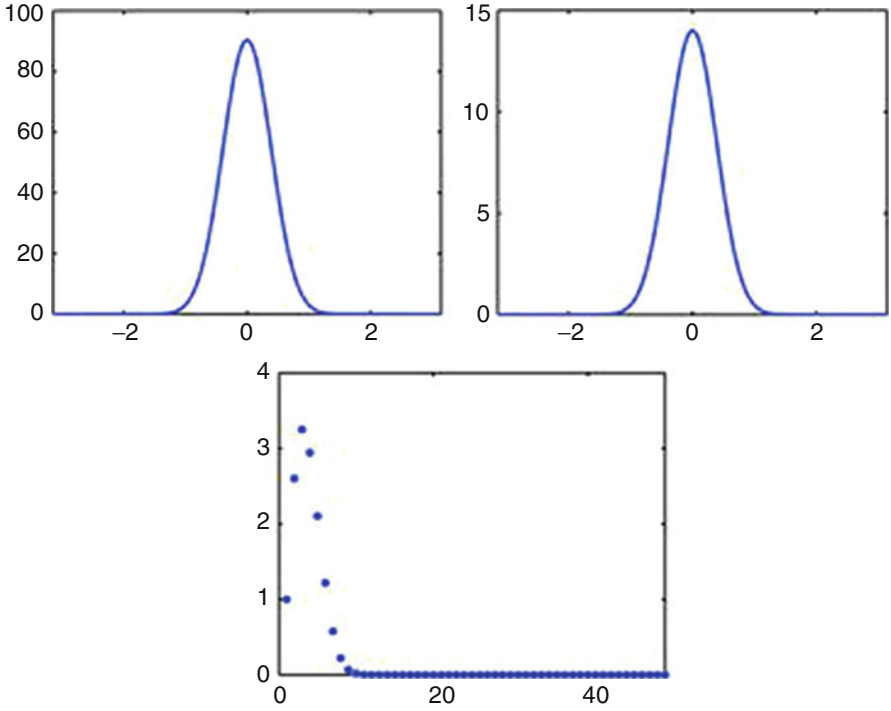

Fig. 1 The de la Vallée Poussin kernel ψ for $\kappa = 7$ its Radon transform $\mathcal{R}\psi$ and its Chebyshev coefficients

Its Radon transform calculates to

$$\mathcal{R}\psi(\mathbf{h}, \mathbf{r}) = \frac{1+\kappa}{2^\kappa}(1 + \mathbf{h} \cdot \mathbf{r})^\kappa = (1+\kappa)\cos^{2\kappa}\eta(\mathbf{h}, \mathbf{r}).$$

The parameter κ controls the halfwidth of the kernel. For illustration, the de la Vallée Poussin kernel ψ, its Radon transform $\mathcal{R}\psi$, and its Chebyshev coefficients $\hat{\psi}$ are plotted in Fig. 1.

6 Texture Analysis with Individual Orientation Measurements: Electron Backscatter Diffraction Data

Electron backscatter diffraction (EBSD) with a scanning electron microscope (SEM) yields Kikuchi patterns (Schwartz et al. 2000), which are "indexed" by advanced image analysis applying Radon and Hough transforms, respectively, to result in individual orientation measurements assigned to locations within the surface of the specimen, i.e., $g_i = g(x_i, y_i), g \in \mathrm{SO}(3), (x_i, y_i) \in D \subset \mathbb{R}^2, i = 1, \ldots, n$. A survey of its application in materials science is given by

Schwartz et al. (2000). Usually, the stepsize of the scanning grid is much smaller than the size of crystallites. Thus, EBSD data are not independent. Since independence and identical distribution are the fundamental assumptions of all classic statistics, proper statistical analysis of EBSD data requires models of spatially induced dependence and methods for dependent data, as developed in Van den Boogaart (2002).

Since density estimation by harmonic series expansion with directly estimated coefficients

$$\hat{f}^*(\ell,k,k') = \frac{1}{n}\frac{(\ell+\frac{1}{2})^{\frac{1}{2}}}{2\pi}\sum_{i=1}^{n}\overline{D_\ell^{kk'}(g_i)}, \ell \in \mathbb{N}_0, k,k' = -\ell,\ldots,\ell \tag{33}$$

is affected by the problem of how to impose non-negativity (Watson 1969), nonparametric kernel density estimation on SO(3) is developed analogously to spherical density estimation (Hall et al. 1987; Schaeben 1982). It may be seen as a convolution of a kernel chosen by the user and the discrete uniform measure assigning to each observation the probability $\frac{1}{n}$, where n denotes the sample size. Any kernel density estimation inevitably involves some smoothing, the extent of the smoothing depending on the width of the kernel, controlled by its parameter κ, or its maximum bandwidth, respectively. In fact, choosing the proper kernel width is critical, much more critical than the choice of the kernel itself (Scott 1992, p. 133). Proceeding from kernel density estimation to estimating the harmonic coefficients may be casually interpreted as smoothing first, then computing harmonic coefficients. Thus, harmonic coefficients determined in this way are generally biased. Only the special case of density estimation with the otherwise unfavorable Dirichlet kernel will yield unbiased estimators of the first L harmonic coefficients.

Let $g_i \in \mathrm{SO}(3), i = 1,\ldots,n$, be a sample of individual orientation measurements of sample size n. Should the measurements initially be spatially referenced, this reference is neglected here. In fact, the sample is modeled as a realization of a mathematical sample of random orientations $G_i : (\Omega, \mathcal{A}, P) \to (\mathrm{SO}(3), \mathcal{B}(\mathrm{SO}(3))), i = 1,\ldots,n$, which are assumed to be independent and identically distributed with finite expectation and finite variance.

Then, the basic kernel density estimator is defined as

$$f_\kappa^*(g; G_1,\ldots,G_n) = \frac{1}{n}\sum_{i=1}^{n}\psi_\kappa(\omega(gG_i^{-1})), \quad \kappa \in \mathbb{A},$$

where $\psi_\kappa, \kappa \in \mathbb{A}$, is a family of non-negative radially symmetric functions, actually an approximate identity for $\kappa \to \kappa_0$. It should be noted that the estimator is a random variable itself. An actual estimate is given by

$$f_\kappa^*(g; g_1,\ldots,g_n) = \frac{1}{n}\sum_{i=1}^{n}\psi_\kappa(\omega(g\, g_i^{-1})), \kappa \in \mathbb{A}.$$

Since it will be clear by the context if the random estimator or its corresponding estimate is meant, they are not distinguished but both denoted f_κ^*.

Considering crystallographic symmetry, the basic kernel density estimator is generalized to

$$\begin{aligned} f_\kappa^*(g; G_1\tilde{G}_{\text{Laue}}, \dots, G_n\tilde{G}_{\text{Laue}}) &= \tfrac{1}{n}\sum_{i=1}^{n} \psi_\kappa\left(\omega\left(g\tilde{G}_{\text{Laue}}G_i^{-1}\right)\right) \\ &= \tfrac{1}{n}\sum_{i=1}^{n} \tfrac{1}{\#\tilde{G}_{\text{Laue}}} \sum_{q\in\tilde{G}_{\text{Laue}}} \psi_\kappa(\omega(gqG_i^{-1})), \quad \kappa \in \mathbb{A}. \end{aligned}$$

As usual, the Radon transform of $f_\kappa^*(g; G_1\tilde{G}_{\text{Laue}}, \dots, G_n\tilde{G}_{\text{Laue}})$ is given by

$$\begin{aligned} \mathcal{R}\left[f_\kappa^*(\circ; G_1\tilde{G}_{\text{Laue}}, \dots, G_n\tilde{G}_{\text{Laue}})\right](\mathbf{h}, \mathbf{r}) &= \tfrac{1}{n}\sum_{i=1}^{n} \mathcal{R}\psi_\kappa(G_i\tilde{G}_{\text{Laue}}\mathbf{h}\cdot\mathbf{r}) \\ &= \tfrac{1}{n}\tfrac{1}{\#\tilde{G}_{\text{Laue}}}\sum_{i=1}^{n} \mathcal{R}\psi_\kappa(G_i\mathbf{h}\cdot\mathbf{r}), \end{aligned}$$

and is itself again a random variable.

Defined as a sum of identical radially symmetric functions, the Fourier coefficients of $f_\kappa^*(g; G_1, \dots, G_n)$ degenerate to the coefficients of the kernel with respect to Chebyshev polynomials of the second kind, Eq. (7), and are given by

$$\begin{aligned} \hat{f}^*(\ell, k, k') &= \frac{\left(\ell + \frac{1}{2}\right)^{\frac{1}{2}}}{2\pi} \int_{\text{SO(3)}} f_\kappa^*(g; G_1, \dots, G_n)\overline{D_\ell^{kk'}(g)\mathrm{d}g} \\ &= \hat{\psi}_\kappa(2\ell)\frac{1}{n}\sum_{i=1}^{n} \overline{D_\ell^{kk'}(G_i)}. \end{aligned}$$

Since smoothing is generally involved in kernel density estimation, the derived estimators of the Radon transform and the harmonic coefficients, respectively, are biased (Van den Boogaart 2002). With respect to the latter, it becomes obvious that the extent of the smoothing (and bias) is captured by the Chebyshev coefficients $\hat{\psi}_\kappa(2\ell)$ of the kernel being used for estimation when the special case of the Dirichlet kernel is being considered.

The Dirichlet kernel $\mathcal{D}_L$ is parametrized by its maximum bandwidth L and defined as

$$\begin{aligned} \mathcal{D}_L(\omega(gg_0^{-1})) &= \sum_{\ell=0}^{L}\sum_{k,k'=-\ell}^{\ell} (2\ell+1) D_\ell^{kk'}(g)\overline{D_\ell^{kk'}(g_0)} \\ &= \sum_{\ell=0}^{L} (2\ell+1)\mathcal{U}_{2\ell}\left(\cos\tfrac{\omega(gg_0^{-1})}{2}\right) \end{aligned}$$

Its Chebyshev coefficients are simply

$$\widehat{\mathcal{D}}_L(2\ell) = \begin{cases} 2\ell + 1, & \text{if } \ell \leq L, \\ 0, & \text{otherwise.} \end{cases} \tag{34}$$

Then, the harmonic coefficients of the Dirichlet kernel density estimator

$$f^*_{\mathcal{D}_L}(g; G_1, \ldots, G_n) = \frac{1}{n} \sum_{i=1}^{n} (2\ell + 1)\mathcal{D}_L \left(\omega \left(g G_i^{-1}\right)\right)$$

are given by

$$\hat{f}^*_{\mathcal{D}_L}(\ell, k, k') = \begin{cases} \hat{f}^*(\ell, k, k'), & \text{if } \ell \leq L, \\ 0, & \text{otherwise,} \end{cases}$$

where $\hat{f}^*(\ell, k, k')$ are the estimators, Eq. (33), directly based on the mathematical sample $G_i, i = 1, \ldots, n$, which have been shown to be unbiased (Van den Boogaart 2002). Here, smoothing of the orientation density function occurs by way of truncation of the harmonic series expansion at the maximum bandwidth L. It could be referred to as computing the harmonic coefficients first, then smoothing the orientation density function by truncation.

Thus, in the special case of nonparametric kernel density estimation with the Dirichlet kernel band-limited by L, the two estimations of the harmonic coefficients coincide for the first L coefficients. Informally, for this special instance, the order of estimation and smoothing is irrelevant. In this way, it is constructively confirmed that the extent of smoothing, which generally accompanies nonparametric kernel density estimation and affects the harmonic coefficients, is obviously captured by the Chebyshev coefficients $\hat{\psi}_\kappa(2\ell)$ of the kernel being used for estimation.

Pursuing the discussion in Watson (1969, 1983), it should be noted that the Dirichlet kernel is not non-negative, cf. Fig. 2, and thus, the corresponding estimated density could be negative. That is, whatever the size of L, the first L unbiased estimates of the harmonic coefficients do not generally represent a non-negative function. Generally, for non-negative kernels, the estimators of the harmonic coefficients are biased. Asymptotically, there is a non-negative density function corresponding to these biased harmonic coefficients. Only for the de la Vallée Poussin kernel, the latter is true for a finite order L, cf. Fengler et al. (2005).

Another quantity of interest is the norm of the estimate or, even more interesting, the expected norm of the estimator. More precisely, the focus is on the asymptotic behavior of the (expected) norm of $f^*_\kappa - f$ for increasingly large sample sizes $n \to \infty$. In particular, the question is how to relate $\kappa \to \kappa_0$ and $n \to \infty$.

Thus, the entity of major interest is the "mean integrated squared error"

$$E\left[\int_{\mathrm{SO}(3)} \left(f^*_\kappa(g; G_1, \ldots, G_n) - f(g)\right)^2 \mathrm{d}g\right]$$

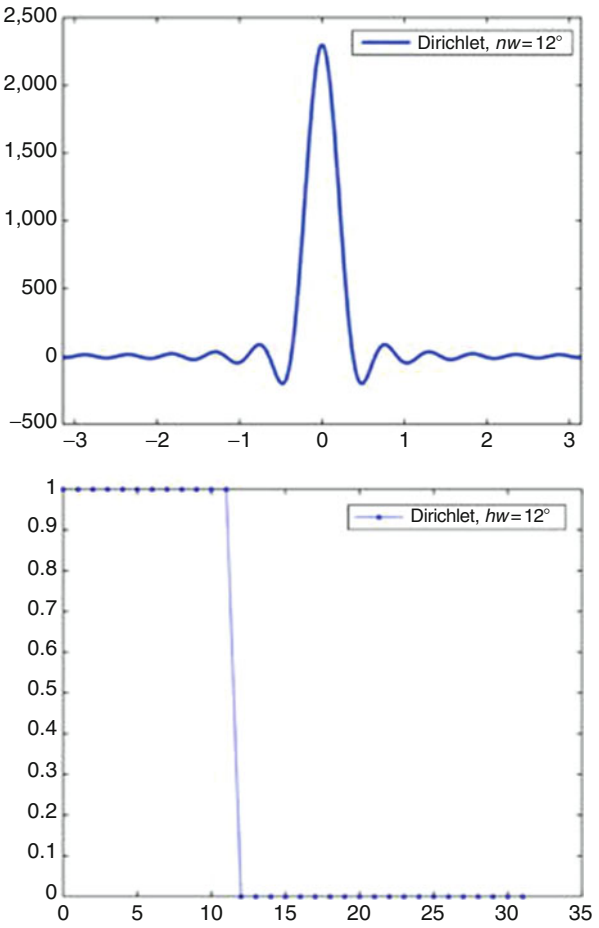

Fig. 2 The Dirichlet kernel $\mathcal{D}_L$ for $L = 11$ and its Chebyshev coefficients

$$= \int_{\mathrm{SO}(3)} E[f_\kappa^*(g; G_1, \ldots, G_n) - f(g)]^2 \mathrm{d}g, \tag{35}$$

which is also the "integrated mean squared error" thanks to Fubini. Thus, it is a measure of both the average global error and the accumulated pointwise error (Scott 1992, p. 38). It is well known that a uniformly minimum-variance unbiased estimator does not exist (Rosenblatt 1956). Therefore, there will always be a trade-off

$$\begin{aligned} &\textstyle\int_{\mathrm{SO}(3)} \mathrm{E}\,[f_\kappa^*(g; G_1, \ldots, G_n) - f(g)]^2 \mathrm{d}g \\ &= \textstyle\int_{\mathrm{SO}(3)} \left(\mathrm{bias}[f_\kappa^*(g; G_1, \ldots, G_n)]\right)^2 \mathrm{d}g + \int_{\mathrm{SO}(3)} \mathrm{Var}\,[f_\kappa^*(g; G_1, \ldots, G_n)]\,\mathrm{d}g \end{aligned} \tag{36}$$

with respect to variance and bias, respectively.

Then, it can be shown that

$$E||f - f_\kappa^*(\circ; G_1, \ldots, G_n)||_{L^2(\mathrm{SO}(3))} = ||f - f * \psi_k||^2_{L^2(\mathrm{SO}(3))} + \tfrac{1}{n}||\psi_\kappa||^2_{L^2(\mathrm{SO}(3))} + \tfrac{1}{n}||f * \psi_k||^2_{L^2(\mathrm{SO}(3))}. \tag{37}$$

While the first term converges for any fixed n to 0 as the kernel ψ_κ approximates identity as $\kappa \to \kappa_0, \kappa \in \mathbb{A}$, the sum of the other two terms essentially depends on the L^2-norm of the kernel and vanishes like $1/n$ for any fixed κ. However, as the kernel approximates identity, its L^2-norm may become arbitrarily large. Thus, a compromise between spatial localization of the kernel controlling the bias term and its L^2-norm is required and will eventually lead to an optimum halfwidth for a given kernel and optimum kernels, respectively, analogously to Epanechnikov (1969).

7 Anisotropic Physical Properties

7.1 Effective Physical Properties of Crystalline Aggregates

Calculation of physical properties from microstructural information (crystal orientation, volume fraction, grain shape, etc.) is important for materials because it gives insight into the role of microstructure in determining bulk properties. Calculation of effective properties is essential for anisotropic properties as experimental measurement in many directions, necessary to fully characterize anisotropy, is not currently feasible for many applications, e.g., in the temperature and pressure conditions found deep in the Earth.

In the following sections, we will only discuss the elastic properties needed for seismic velocities, but the methods apply to all tensorial properties where the bulk property is governed by the volume fraction of the constituent minerals. Many properties of geophysical interest are of this type, e.g., thermal conductivity, thermal expansion, elasticity, and seismic velocity. However, these methods do not apply to properties determined by the connectivity of a phase, such as the electrical conductivity of rocks with conductive films on grain boundaries (e.g., carbon). We will assume that the sample may be microscopically heterogeneous due to grain size, shape, orientation, or phase distribution but will be considered macroscopically uniform. The complete structural details of the sample are in general never known, but a "statistically uniform" sample contains many regions, which are compositionally and structurally similar, each fairly representative of the entire sample. The local stress and strain fields at every point $\mathbf{r}$ in a linear elastic polycrystal are completely determined by Hooke's law as follows:

$$\sigma_{ij}(\mathbf{r}) = C_{ijkl}(\mathbf{r})\epsilon_{kl}(\mathbf{r}),$$
$$\epsilon_{ij}(\mathbf{r}) = S_{ijkl}(\mathbf{r})\sigma_{kl}(\mathbf{r}),$$

where $\sigma_{ij}(\mathbf{r})$ is the stress tensor, $\varepsilon_{kl}(\mathbf{r})$ is the strain tensor, $C_{ijkl}(\mathbf{r})$ is the elastic stiffness tensor, and $S_{ijkl}(\mathbf{r})$ is the elastic compliance tensor at point $\mathbf{r}$. The evaluation of the effective constants of a polycrystal would be the summation of all components as a function of position if we know the spatial functions of stress and strain. The average stress $< \sigma_{ij} >$ and strain $< \varepsilon_{ij} >$ of a statistically uniform sample are linked by effective macroscopic moduli C^* and S^* that obey Hookes's law of linear elasticity,

$$\begin{aligned} C^*_{ijkl} &= < \sigma_{ij} >< \epsilon_{kl} >^{-1}, \\ S^*_{ijkl} &= < \epsilon_{ij} >< \sigma_{kl} >^{-1}, \end{aligned}$$

where $< \epsilon_{ij} >= \frac{1}{V}\int \epsilon_{ij}(\mathbf{r})\mathrm{d}r$, $< \sigma_{ij} >= \frac{1}{V}\int \sigma_{ij}(\mathbf{r})\mathrm{d}r$, V is the volume, and the notation $< . >$ denotes an ensemble average. The stress $\sigma(\mathbf{r})$ and strain $\varepsilon(\mathbf{r})$ distribution in a real polycrystal vary discontinuously at the surface of grains. By replacing the real polycrystal with a "statistically uniform" sample, we are assuming that stress $\sigma(\mathbf{r})$ and strain $\varepsilon(\mathbf{r})$ are varying slowly and continuously with position $\mathbf{r}$.

A number of methods are available for determining the effective macroscopic modulus of an aggregate. We make the simplifying assumption that there is no significant interaction between grains, which for fully dense polycrystalline aggregates is justified by agreement between theory and experiments for the methods we present here. However, these methods are not appropriate for aggregates that contain voids, cracks, or pores filled with liquids or gases, as the elastic contrast between the different microstructural elements will be too high and we cannot ignore elastic interactions in such cases. The classical method that takes into account grain interaction is the self-consistent method based on the Eshelby inclusion model (e.g., Eshelby 1957; Hill 1965, which can also account for the shape of the microstructural elements. The simplest and best-known averaging techniques for obtaining estimates of the effective elastic constants of polycrystals are the Voigt (1928) and Reuss (1929) averages. These averages only use the volume fraction of each phase, the orientation, and the elastic constants of the single crystals or grains. In terms of statistical probability functions, these are first-order bounds, as only the first-order correlation function is used, which is the volume fraction. Note that no information about the shape or position of neighboring grains is used. The Voigt average is found by simply assuming that the strain field is everywhere constant (i.e., $\varepsilon(\mathbf{r})$ is independent of $\mathbf{r}$) and hence the strain is equal to its mean value in each grain. The strain at every position is set equal to the macroscopic strain of the sample. C^* is then estimated by a volume average of local stiffnesses $C(g_i)$ with orientation g_i and volume fraction V_i,

$$C^* \approx C^{\mathrm{Voigt}} = \left[\sum_i V_i C(g_i)\right].$$

The Reuss average is found by assuming that the stress field is everywhere constant. The stress at every position is set equal to the macroscopic stress of the sample. C^* or S^* is then estimated by the volume average of local compliances $S(g_i)$,

$$\begin{aligned} C^* &\approx C^{\text{Reuss}} = \left[\sum_i V_i S(g_i)\right]^{-1} \\ S^* &\approx S^{\text{Reuss}} = \left[\sum_i V_i S(g_i)\right] \end{aligned} .$$

and

$$C^{\text{Voigt}} \neq C^{\text{Reuss}} \text{ and } C^{\text{Voigt}} \neq [S^{\text{Reuss}}]^{-1}.$$

These two estimates are not equal for anisotropic solids, with the Voigt being an upper bound and the Reuss a lower bound. A physical estimate of the moduli should lie between the Voigt and Reuss average bounds, as the stress and strain distributions are expected to be somewhere between uniform strain (Voigt bound) and uniform stress (Reuss bound). Hill (1952) observed that the arithmetic mean (and the geometric mean) of the Voigt and Reuss bounds, sometimes called the Hill or Voigt-Reuss-Hill (VRH) average, is often close to experimental values. The VRH average has no theoretical justification. As it is much easier to calculate the arithmetic mean of the Voigt and Reuss elastic tensors, all authors have tended to apply the Hill average as an arithmetic mean. In Earth sciences, the Voigt, Reuss, and Hill averages have been widely used for averages of oriented polyphase rocks (e.g., Crosson and Lin 1971). Although the Voigt and Reuss bounds are often far apart for anisotropic materials, they still provide the limits within which the experimental data should be found.

Several authors have searched for a geometric mean of oriented polycrystals using the exponent of the average of the natural logarithms of the eigenvalues of the stiffness matrix (Matthies and Humbert 1993). Their choice of this averaging procedure was guided by the fact that the ensemble average elastic stiffness $< C >$ should equal the inverse of the ensemble average elastic compliances $< S >^{-1}$, which is not true, for example, of the Voigt and Reuss estimates. A method of determining the geometric mean for arbitrary orientation distributions has been developed (Matthies and Humbert 1993). The method derives from the fact that a stable elastic solid must have an elastic strain energy that is positive. It follows from this that the eigenvalues of the elastic matrix must all be positive. Comparison between Voigt, Reuss, Hill, and self-consistent estimates shows that the geometric mean provides estimates very close to the self-consistent method but at considerably reduced computational complexity (Matthies and Humbert 1993). The condition that the macroscopic polycrystal elastic stiffness $< C >$ must equal the inverse of the aggregate elastic compliance $< S >^{-1}$ would appear to be a powerful physical constraint on the averaging method (Matthies and Humbert 1993). However, the arithmetic (Hill) and geometric means are also very similar

(Mainprice and Humbert 1994), which tends to suggest that they are just mean estimates with no additional physical significance.

The fact that there is a wide separation between the Voigt and Reuss bounds for anisotropic materials is caused by the fact that the microstructure is not fully described by such averages. However, despite the fact that these methods do not take into account such basic information as the position or the shape of grains, several studies have shown that the Voigt and Hill average are within 5–10 % of experimental values for crystalline rocks. For example, Barruol and Kern (1996) showed for several anisotropic lower-crust and upper-mantle rocks from the Ivrea zone in Italy that the Voigt average is within 5 % of the experimentally measured velocity.

7.2 Properties of Polycrystalline Aggregates with Texture

The orientation of crystals in a polycrystal can be measured by volume diffraction techniques (e.g., X-ray or neutron diffraction) or individual orientation measurements (e.g., U-stage and Optical microscope, electron channeling, or electron backscattered diffraction (EBSD)). In addition, numerical simulations of polycrystalline plasticity also produce populations of crystal orientations at mantle conditions (e.g., Tommasi et al. 2004). An orientation, often given the letter g, of a grain or crystal in sample coordinates can be described by the rotation matrix between crystal and sample coordinates. In practice, it is convenient to describe the rotation by a triplet of Euler angles, e.g., $g = (\phi_1, \Phi, \phi_2)$ by Bunge (1982). One should be aware that there are many different definitions of Euler angles that are used in the physical sciences. The orientation distribution function (O.D.F.) $f(g)$ is defined as the volume fraction of orientations, with an orientation in the interval between g and $g + \mathrm{d}g$ in a space containing all possible orientations given by

$$\frac{\Delta V}{V} = \int f(g)\mathrm{d}g,$$

where $\Delta V/V$ is the volume fraction of crystals with orientation g, $f(g)$ is the texture function, and $\mathrm{d}g = 1/8\pi^2 \sin\varphi \ \mathrm{d}\phi_1 \ \mathrm{d}\Phi \ \mathrm{d}\phi_2$ is the volume of the region of integration in orientation space.

To calculate the seismic properties of a polycrystal, one must evaluate the elastic properties of the aggregate. In the case of an aggregate with a crystallographic texture, the anisotropy of the elastic properties of the single crystal must be taken into account. A potential complication is the fact that the Cartesian frame defined by orthogonal crystallographic directions used report elastic tensor of the single crystal, may not be the same as those used for Euler angle reference frame used in texture analysis (e.g., MTEX) or measurement (e.g., EBSD) packages. To account for this difference, a rotation may be required to bring the crystallographic frame of tensor into coincidence with the Euler angle frame,

$$C_{ijkl}(g^{\mathrm{E}}) = T_{ip}.T_{jq}.T_{kr}.T_{lt}C_{pqrt}(g^{\mathrm{T}}),$$

where $C_{ijkl}(g^E)$ is the elastic property in the Euler reference and $C_{pqrt}\ (g^T)$ is the elastic property in the original tensor reference frame; both frames are in crystal coordinates. The transformation matrix T_{ij} is constructed from the angles between the two sets perpendicular to the crystallographic axes, forming rows and columns of the orthogonal transformation or rotation matrix (see Nye 1957). For each orientation g, the single-crystal properties have to be rotated into the specimen coordinate frame using the orientation or rotation matrix g_{ij},

$$C_{ijkl}(g) = g_{ip}.g_{jq}.g_{kr}.g_{lt}.C_{pqrt}(g^{\mathrm{E}}),$$

where $C_{ijkl}(g^E)$ is the elastic property in sample coordinates, $g_{ij} = g(\phi_1, \Phi, \phi_2)$ is the measured orientation in sample coordinates, and $C_{pqrt}\ (g^E)$ is the elastic property in crystal coordinates of the Euler frame. We can rewrite the above equation as

$$C_{ijkl}(g) = T_{ijklpqrt}(g)C_{pqrt}(g^{\mathrm{E}})$$

with

$$T_{ijklpqrt}(g) = \partial x_i/\partial x_p \partial x_j/\partial x_q \partial x_k/\partial x_r \partial x_l/\partial x_t = g_{ip}.g_{jq}.g_{kr}.g_{lt}.$$

The elastic properties of the polycrystal may be calculated by integration over all possible orientations of the ODF. Bunge (1982) has shown that integration is given as

$$< C_{ijkl} >= \int g_{ip}.g_{jq}.g_{kr}.g_{lt}.C_{pqrt}(g^E).f(g)\ \mathrm{d}g = \int C_{ijkl}(g).f(g)\ \mathrm{d}g,$$

where $< C_{ijkl} >$ are the elastic properties of the aggregate and $\int f(g)\mathrm{d}g = 1$. The integral on SO(3) can be calculated efficiently using the numerical methods available in MTEX.

We can also regroup the texture-dependent part of the integral as $< T_{ijklpqrt} >$

$$< T_{ijklpqrt} > \cdot C_{pqrt}(g^{\mathrm{E}}) = \left[\int T_{ijklpqrt}(g) \cdot f(g)dg\right] \cdot C_{pqrt}(g^{\mathrm{E}}).$$

We can evaluate $< T_{ijklpqrt} >$ analytically in terms of generalized spherical harmonic coefficients for specific crystal and sample symmetries (e.g., Ganster and Geiss 1985; Johnson and Wenk 1986; Morris 2006; Zuo et al. 1989). The minimum texture information required to calcluate the elastic properties are the even-order coefficients and series expansion to 4, which drives from centrosymmetric symmetry and fourth-rank tensor of elasticity, respectively. The direct consequence of this is

that only a limited number of pole figures are required to define the ODF, e.g., 1 for cubic and hexagonal and 2 for tetragonal and trigonal crystal symmetries.

Alternatively, elastic properties may be determined by simple summation of individual orientation measurements

$$< C_{ijkl} >= \sum g_{ip}.g_{jq}.g_{kr}.g_{lt}.C_{pqrt}(g^{\mathrm{E}}).V(g) = \sum C_{ijkl}(g).V(g),$$

where $V(g)$ is the volume fraction of grains in orientation g. For example, the Voigt average of the rock for m mineral phases of volume fraction $V(m)$ is given as

$$< C_{ijkl} >^{\mathrm{Voigt}} = \sum V(m) < C_{ijkl} >^{m}.$$

The final step is the calculation of the three seismic phase velocities by solution of the Christoffel tensor (T_{ik}). The Christoffel tensor is symmetrical because of the symmetry of the elastic constants, and hence,

$$T_{ik} = C_{ijkl}n_j n_l = C_{jikl}n_j n_l = C_{ijlk}n_j n_l = C_{klij}n_j n_l = T_{ki}.$$

The Christoffel tensor is also invariant upon the change of sign of the propagation direction **n**, as the elastic tensor is not sensitive to the presence or absence of a center of symmetry, being a centrosymmetric physical property. Because the elastic strain energy $\left(\frac{1}{2}C_{ijkl}\epsilon_{ij}\epsilon_{kl}\right)$ of a stable crystal is always positive and real (e.g., Nye 1957), the eigenvalues of the 3×3 Christoffel tensor (being a Hermitian matrix) are three positive real values of the wave moduli M corresponding to ρVp^2, ρVs_1^2, and ρVs_2^2 of the plane waves propagating in the direction **n**. The three eigenvectors of the Christoffel tensor are the polarization directions (also called vibration, particle movement, or displacement vectors) of the three waves, as the Christoffel tensor is symmetrical to the three eigenvectors, and polarization vectors are mutually perpendicular. In the most general case, there are no particular angular relationships between polarization directions **p** and the propagation direction **n**; however, typically the P-wave polarization direction is nearly parallel and the two S-wave polarizations are nearly perpendicular to the propagation direction, and they are termed quasi-P or quasi-S waves. If the P-wave and two S-wave polarizations are parallel and perpendicular to the propagation direction, which may happen along a symmetry direction, then the waves are termed pure P and pure S or pure modes. In general, the three waves have polarizations that are perpendicular to one another and propagate in the same direction with different velocities, with $Vp > Vs_1 > Vs_2$.

7.3 Properties of Polycrystalline Aggregates: An Example

Metamorphic reactions and phase transformations often result in specific crystallographic relations between minerals. A specific orientation relationship between two minerals is defined by choosing any orientation descriptor that is convenient,

e.g., a pair of parallel crystallographic features, Euler angle triplet, rotation matrix, or rotation axis and angle. The two minerals may have the same or different crystal symmetries. The composition may be the same, as in polymorphic phase transitions, or different, as in dehydration or oxidization reactions. Recently, Boudier et al. (2009) described the orientation relationship between olivine and antigorite serpentine crystal structures by two pairs of planes and directions that are parallel in both minerals:

relation 1 : (100) Olivine||(001)Antigorite and[001]Olivine||[010]Antigorite
relation 2 : (010) Olivine||(001)Antigorite and[001]Olivine||[010]Antigorite

Such relationships are called Burgers orientation relationships in metallurgy. The relation is used in the present study to calculate the Euler angle triplet, which characterizes the rotation of the crystal axes of antigorite into coincidence with those of olivine. Olivine is hydrated to form antigorite, and in the present case, the rotational point group symmetry of olivine (orthorhombic) and antigorite (monoclinic) results in four symmetrically equivalent new mineral orientations (see Mainprice et al. (1990) for details) because of the symmetry of the olivine that is transformed. The orientation of the n symmetrically equivalent antigorite minerals is given by

$$g^{\text{Antigorite}}_{n=1,\ldots,4} = \Delta g^{\text{Olivine}-\text{Antigorite}}.S^{\text{Olivine}}_{\text{n}}.g^{\text{Olivine}},$$

where $\Delta g^{\text{Olivine}-\text{Antigorite}}$ is rotation between olivine and newly formed antigorite, S^{Olivine}_{n} are the rotational point group symmetry operations of olivine, and g^{Olivine} is the orientation of an olivine crystal. Δg is defined by the Burgers relationships given above, where relation 1 is $\Delta g = \phi_1, \Phi, \phi_2 = (88.6, 90.0, 0.0)$ and relation 2 is $\Delta g = (178.6, 90.0, 0.0)$. Note that the values of the Euler angles of Δg will depend on the right-handed orthonormal crystal coordinate system chosen for the orthorhombic olivine and the monoclinic antigorite. In this example, for olivine $\mathcal{K}_C = \{\mathbf{a}, \mathbf{b}, \mathbf{c}\}$, and for antigorite $\mathcal{K}_C = \{\mathbf{a}*, \mathbf{b}, \mathbf{c}\}$.

The measurement of the texture of antigorite is often unreliable using EBSD because of sample preparation problems. We will use Δg, which may be expressed as a mineral or phase misorientation function (Bunge and Weiland 1988) as

$$F^{\text{Olivine}-\text{Antigorite}}(\Delta g) = \int f^{\text{Olivine}}(g).f^{\text{Antigorite}}(\Delta g.g)\mathrm{d}g$$

to predict the texture of antigorite from the measured texture of olivine. We will only use relation 1 of Boudier et al. (2009) because this relation was found to have a much higher frequency in their samples. We used the olivine texture database of Ben Ismail and Mainprice (1998), consisting of 110 samples and over 10,000 individual measurements made with an optical microscope equipped with a five axis universal stage as our model olivine texture illustrated in Fig. 3. The olivine model texture has the [100] aligned with the lineation and the [010] axes normal to the foliation.

The texture of the antigorite, calculated using phase misorientation functions, and the pole figures (Fig. 3) clearly show that Burgers orientation relationships between olivine and antigorite are statistically respected in the aggregates. The seismic properties of the 100 % olivine and antigorite aggregates were calculated using the methods described in Sect. 6.2 for individual orientations using the elastic single-crystal tensors for olivine (Abramson et al. 1997) and antigorite (Pellenq et al. 2009), respectively. The numerical methods for the seismic calculations are described by Mainprice (1990). The seismic velocities for a given propagation direction are on a five degree grid in the lower hemisphere. The percentage anisotropy (A) is defined here as $A = 200(V_{\max} - V_{\min})/(V_{\max} + V_{\min})$. The V_p anisotropy is found by searching the hemisphere for all possible propagation directions for maximum and minimum values of V_p. There are in general two orthogonally polarized S-waves for each propagation direction with different velocities in an anisotropic medium. The anisotropy *AVs* can then be defined for each direction, with one S-wave having the maximum velocity and the other the minimum velocity. Contoured lower-hemisphere stereograms of P-wave velocity (V_p), percentage shear-wave anisotropy (*AVs*), also called shear-wave splitting, as well as polarization (Vs_1) of the fastest S-wave are shown in Fig. 4. The seismic properties show a major change in the orientation of the fast direction of compressional wave propagation from parallel to the lineation (X) in the olivine aggregate to normal to the foliation (Z) in the antigorite aggregate. In addition, there is a dramatic change of orientation of the polarization (or vibration) of the fastest S-wave (S1) from parallel to the (XY) foliation plane in the olivine aggregate to perpendicular to the foliation (Z) in the antigorite aggregate. The remarkable changes in seismic properties associated with hydration of olivine and its transformation to antigorite have been invoked to explain the changes in orientation of S-wave polarization of the upper mantle between back arc and mantle wedge in subduction zones (Faccenda et al. 2008; Katayama et al. 2009; Kneller et al. 2008).

8 Future Directions

Although quantitative texture analysis has been formally available since the publication of the H.-J. Bunges classical book (1969), many of the original concepts only applied to single-phase aggregates of metals. Extension of these methods was rapidly made to lower crystal symmetry typical of rock-forming minerals and lower sample symmetry corresponding to naturally deformed rocks. The relationship of neighboring crystal orientations called misorientation has also now been widely studied. However, most rocks are poly mineral or poly phase, and the extension of quantitative texture analysis to poly phase materials has been slow to develop because a universal mathematical framework is missing. A coherent framework will encompass misorientation between crystals of the same phase and between crystals of different phases. Future research in this area based on the mathematical framework of this chapter will provide a coherent and efficient theoretical and numerical methodology. Other future developments will include

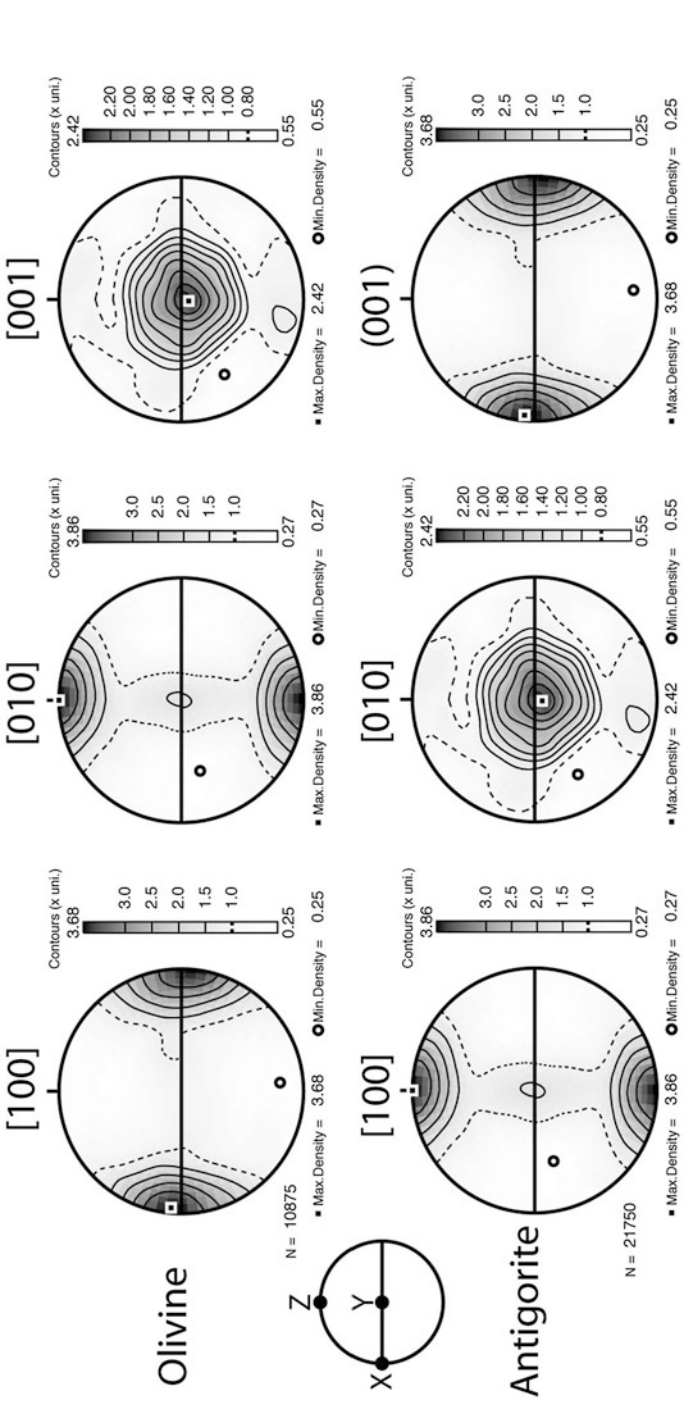

Fig. 3 Olivine CPO of the Ben Ismail and Mainprice (1998) database and the corresponding antigorite CPO calculated using phase misorientation function described in the text. *Horizontal black lines* on the pole figures marks the foliation (XY) plane of the olivine aggregates and the lineation (X) is East-West. Contours in times uniform. Lower hemisphere equal area projection

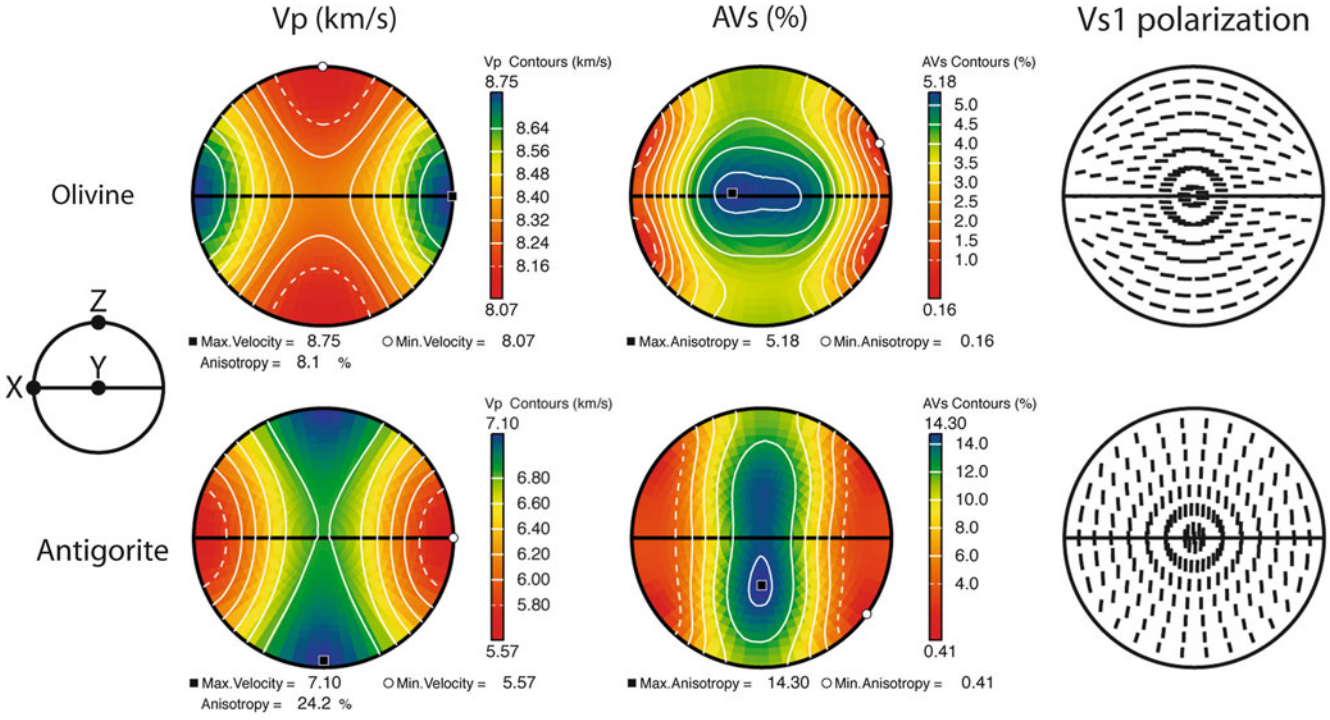

Fig. 4 The calculated seismic properties of the olivine and antigorite polycrystals with pole figures shown in Fig. 3. V_p is compression wave velocity, *AVs* is shear-wave splitting or birefringence anisotropy as percentage as defined in the text and Vs_1 polarization is the vibration direction of the fastest S-wave. *Horizontal black lines* on the pole figures marks the foliation (*XY*) plane of the olivine aggregates and the lineation (*X*) is East-West. Lower hemisphere equal area projection

methods to quantify the statistical sampling of the orientation space of different types of data.

9 Conclusions

Forty years after Bunge's pioneering *Mathematische Methoden der Texturanalyse* (Bunge 1969), which is most likely the single most influential textbook besides its English translation (Bunge 1982), this contribution to the *Handbook of Geomathematics* presents elements of mathematical texture analysis as part of mathematical tomography. The "fundamental relationship" of an orientation distribution and its corresponding "pole figures" was identified as a totally geodesic Radon transform on SO(3) or $\mathbb{S}^3 \subset \mathbb{H}$. Being a Radon transform, pole figures are governed by an ultrahyperbolic or Darboux-type differential equation, the meaning of which was furiously denied at its first appearance. In fact, this differential equation opened a new dimension, and its general solution, both in terms of harmonics and characteristics, suggested a novel approach by radial basis functions, featuring a compromise of sufficiently good localization in spatial and frequency domains. Availability of fast Fourier methods for spheres and SO(3) was the necessary prerequiste to put the mathematics of texture analysis into practice, as provided by the free and open-source toolbox MTEX.

References

Abramson EH, Brown JM, Slutsky LJ, Zaug J (1997) The elastic constants of San Carlos olivine to 17 GPa. J Geophys Res 102:12253–12263

Altmann SL (1986) Rotations, quaternions and double groups. Clarendon, Oxford

Barruol G, Kern H (1996) P and S waves velocities and shear wave splitting in the lower crustal/upper mantle transition (Ivrea Zone). Experimental and calculated data. Phys Earth Planet Int 95:175–194

Ben Ismail W, Mainprice D (1998) An olivine fabric database: an overview of upper mantle fabrics and seismic anisotropy. Tectonophysics 296:145–157

Bernier JV, Miller MP, Boyce DE (2006) A novel optimization-based pole-figure inversion method: comparison with WIMV and maximum entropy methods. J Appl Cryst 39:697–713

Bernstein S, Schaeben H (2005) A one-dimensional radon transform on SO(3) and its application to texture goniometry. Math Methods Appl Sci 28:1269–1289

Bernstein S, Hielscher R, Schaeben H (2009) The generalized totally geodesic Radon transform and its application in texture analysis. Math Methods Appl Sci 32:379–394

Boudier F, Baronnet A, Mainprice D (2009) Serpentine mineral replacements of natural olivine and their seismic implications: oceanic lizardite versus subduction-related antigorite. J Pet. doi:10.1093/petrology/egp049

Bunge HJ (1965) Zur Darstellung allgemeiner Texturen. Z Metallk 56:872–874

Bunge HJ (1969) Mathematische Methoden der Texturanalyse. Akademie-Verlag, New York

Bunge HJ (1982) Texture analysis in materials science. Butterworths, Boston

Bunge HJ, Weiland H (1988) Orientation correlation in grain and phase boundaries. Textures Microstruct 7:231–263

Cowley JM (1995) Diffraction physics, 3rd edn. North-Holland personal library. North-Holland, Oxford

Crosson RS, Lin JW (1971) Voigt and Reuss prediction of anisotropic elasticity of dunite. J Geophys Res 76:570–578
Epanechnikov VA (1969) Nonparametric estimates of a multivariate probability density. Theor Probl Appl 14:153–158
Eshelby JD (1957) The determination of the elastic field of a ellipsoidal inclusion, and related problems. Proc R Soc Lond A 241:376–396
Faccenda M, Burlini L, Gerya T, Mainprice D (2008) Fault-induced seismic anisotropy by hydration in subducting oceanic plates. Nature 455:1097–1101
Fengler MJ, Freeden W, Gutting M (2006) The Spherical Bernstein Wavelet. Int J Pure Appl Math, 31, 209–230
Forsyth JB (1988) Single crystal diffractometry. In: Newport RJ, Rainford BD, Cywinski R (eds) Neutron scattering at a pulsed source. Adam Hilger, Bristol, pp 177–188
Friedel G (1913) Sur les symetries cristallines que peut reveler la diffraction des rayons Röntgen. C R Acad Sci 157:1533–1536
Ganster J, Geiss D (1985) Polycrystalline simple average of mechanical properties in the general (triclinic) case. Phys Stat Sol (B) 132:395–407
Gel'fand IM, Minlos RA, Shapiro ZYa (1963) Representations of the rotation and Lorentz groups and their application. Pergamon, Oxford
Gürlebeck K, Sprößig W (1997) Quaternionic and Clifford calculus for physicists and engineers. Wiley, New York
Hall P, Watson GS, Cabrera J (1987) Kernel density estimation with spherical data. Biometrika 74:751–762
Hammond C (1997) The basics of crystallography and diffraction. Oxford University Press, Oxford
Hanson AJ (2006) Visualizing quaternions. Morgan Kaufmann, San Francisco
Helgason S (1984) Groups and geometric analysis. Academic, New York/Orlando
Helgason S (1994) Geometric analysis on symmetric spaces. Mathematical surveys and monographs, vol 39. American Mathematical Society, New York/Orlando
Helgason S (1999) The Radon transform, 2nd edn. Birkhäuser Boston, Boston
Hielscher R (2007) The Radon transform on the rotation group-inversion and application to texture analysis. PhD thesis, TU Bergakademie Freiberg
Hielscher R, Schaeben H (2008a) A novel pole figure inversion method: specification of the MTEX algorithm. J Appl Cryst 41:1024–1037
Hielscher R, Schaeben H (2008b) MultiScale texture modeling. Math Geosci 40:63–82
Hielscher R, Potts D, Prestin J, Schaeben H, Schmalz M (2008) The Radon transform on SO(3): a Fourier slice theorem and numerical inversion. Inverse Probl 24:025011 (21p)
Hielscher R, Prestin J, Vollrath A (2010) Fast summation of functions on SO(3). Math Geosci, 42, 773–794
Hill R (1952) The elastic behaviour of a crystalline aggregate. Proc Phys Soc Lond Ser A 65:349–354
Hill R (1965) A self consistent mechanics of composite materials. J Mech Phys Solids 13:213–222
Johnson GC, Wenk HR (1986) Elastic properties of polycrystals with trigonal crystal and orthorhombic specimen symmetry. J Appl Phys 60:3868–3875
Katayama I, Hirauchi KI, Michibayashi K, Ando JI (2009) Trench-parallel anisotropy produced by serpentine deformation in the hydrated mantle wedge. Nature 461:1114–1118. doi:10.1038/nature08513
Kneller EA, Long MD, van Keken PE (2008) Olivine fabric transitions and shear wave anisotropy in the Ryukyu subduction system. Earth Planet Sci Lett 268:268–282
Kostelec PJ, Rockmore DN (2003) FFTs on the rotation group. Santa Fe institute working papers series paper, 03-11-060
Kreminski R (1997) Visualizing the Hopf fibration. Math Educ Res 6:9–14
Kuipers JB (1999) Quaternions and rotation sequences-a primer with applications to orbits, aerospace, and virtual reality. Princeton University Press, Princeton
Kunze K (1991) Zur quantitativen Texturanalyse von Gesteinen: Bestimmung, Interpretation und Simulation von Quarztefügen. PhD thesis, RWTH Aachen

Kunze K, Schaeben H (2004) The Bingham distribution of rotations and its spherical Radon transform in texture analysis. Math Geol 36:917–943
Mainprice D (1990) A FORTRAN program to calculate seismic anisotropy from the lattice preferred orientation of minerals. Comput Geosci 16:385–393
Mainprice D, Humbert M (1994) Methods of calculating petrophysical properties from lattice preferred orientation data. Surv Geophys 15:575–592 (Special Issue Seismic properties of crustal and mantle rocks: laboratory measurements and theoretical calculations)
Mainprice D, Humbert M, Wagner F (1990) Phase transformations and inherited lattice preferred orientation: implications for seismic properties. Tectonophysics 180:213–228
Mainprice D, Tommasi A, Couvy H, Cordier P, Frost DJ (2005) Pressure sensitivity of olivine slip systems: implications for the interpretation of seismic anisotropy of the Earths upper mantle. Nature 433:731–733
Mao HK, Shu J, Shen G, Hemley RJ, Li B, Singh, AK (1998) Elasticity and rheology of iron above 220 GPa and the nature of the Earths inner core. Nature 396:741–743
Matthies S (1979) On the reproducibility of the orientation distribution function of texture samples from pole figures (ghost phenomena). Phys Stat Sol (B) 92:K135–K138
Matthies S, Humbert M (1993) The realization of the concept of a geometric mean for calculating physical constants of polycrystalline materials. Phys Stat Sol (B) 177:K47–K50
Matthies S, Vinel GW, Helming K (1987) Standard distributions in texture analysis, vol I. Akademie Verlag, New York
Meister L, Schaeben H (2004) A concise quaternion geometry of rotations. Math Methods Appl Sci 28:101–126
Morawiec A (2004) Orientations and rotations. Springer, Berlin
Morris PR (2006) Polycrystal elastic constants for triclinic crystal and physical symmetry. J Appl Cryst 39:502–508. doi:10.1107/S002188980 6016645
Muller J, Esling C, Bunge HJ (1981) An inversion formula expressing the texture function in terms of angular distribution function. J Phys 42:161–165
Nye JF (1957) Physical properties of crystals – their representation by tensors and matrices. Oxford University Press, Oxford
Nikiforov AF, Uvarov VB (1988) Special functions in mathematical physics. Birkhäuser Boston, Boston
Nikolayev DI, Schaeben H (1999) Characteristics of the ultrahyperbolic differential equation governing pole density functions. Inverse Probl 15:1603–1619
Pellenq RJM, Mainprice D, Ildefonse B, Devouard B, Baronnet A, Grauby O (2009) Atomistic calculations of the elastic properties of antigorite at upper mantle conditions: application to the seismic properties in subduction zones. EPSL submitted
Prior DJ, Mariani E, Wheeler J (2009) EBSD in the Earth Sciences: applications, common practice and challenges. In: Schwartz AJ, Kumar M, Adams BL, Field DP (eds) Electron backscatter diffraction in materials science. Springer, Berlin
Randle V, Engler O (2000) Texture analysis: macrotexture, microtexture, and orientation mapping. Gordon and Breach Science, New York
Raterron P, Merkel S (2009) In situ rheological measurements at extreme pressure and temperature using synchrotron X-ray diffraction and radiography. J Synchrotron Radiat 16:748–756
Reuss A (1929) Berechnung der Fließgrenze von Mischkristallen auf Grund der Plastizitätsbedingung für Einkristalle. Z Angew Math Mech 9:49–58
Roe RJ (1965) Description of crystallite orientation in polycrystal materials III. General solution to pole figure inversion. J Appl Phys 36:2024–2031
Rosenblatt M (1956) Remarks on some nonparametric estimates of a density function. Ann Math Stat 27:832–837
Sander B (1930) Gefügekunde der Gesteine mit besonderer Bercksichtigung der Tektonite. Springer, Berlin, p 352
Savyolova TI (1994) Inverse formulae for orientation distribution function. Bunge HJ (ed) Proceedings of the tenth international conference on textures of materials (Materials Science Forum 15762), pp 419–421

Schaeben H (1982) Fabric-diagram contour precision and size of counting element related to sample size by approximation theory methods. Math Geol 14:205–216 [Erratum: Math Geol 15:579–580]
Schaeben H (1997) A simple standard orientation density function: the hyperspherical de la Vallée Poussin kernel. Phys Stat Sol (B) 200:367–376
Schaeben H (1999) The de la Vallée Poussin standard orientation density function. Textures Microstruct 33:365–373
Schaeben H, Sprößig W, van den Boogaart KG (2001) The spherical X-ray transform of texture goniometry. In: Brackx F, Chisholm JSR, Soucek V (eds) Clifford analysis and its applications. Proceedings of the NATO advanced research workshop Prague, 30 Oct–3 Nov, 2000, pp 283–291
Schaeben H, Hielscher R, Fundenberger, J-J, Potts D, Prestin J (2007) Orientation density function-controlled pole probability density function measurements: automated adaptive control of texture goniometers. J Appl Cryst 40:570–579
Schwartz AJ, Kumar M, Adams BL (2000) Electron back scatter diffraction in materials science. Kluwer Academic, Dordrecht
Scott DW (1992) Multivariate density estimation-Theory, practice, and visualization. Wiley, New York
Tommasi A, Mainprice D, Cordier P, Thoraval C, Couvy H (2004) Strain-induced seismic anisotropy of wadsleyite polycrystals: constraints on flow patterns in the mantle transition zone. J Geophys Res 109:B12405, 1–10
Vajk KM (1995) Spin space and the strange properties of rotations. MSc thesis, UC Santa Cruz
Van den Boogaart KG (2002) Statistics for Individual Crystallographic Orientation Measurements. PhD thesis, TU Bergakademie Freiberg
Van den Boogaart KG, Hielscher R, Prestin J, Schaeben H (2007) Kernel-based methods for inversion of the Radon transform on SO(3) and their applications to texture analysis. J Comput Appl Math 199:122–140
Van Houtte P (1980) A method for orientation distribution function analysis from incomplete pole figures normalized by an iterative method. Mater Sci Eng 43:7–11
Van Houtte P (1984) A new method for the determination of texture functions from incomplete pole figures – comparison with older methods. Textures Microstruct 6:137–162
Varshalovich D, Moskalev A, Khersonski V (1988) Quantum theory of angular momentum. World Scientific, Singapore
Vilenkin NJ (1968) Secial functions and the theory of group representations. American Mathematical Society, Providence
Vilenkin NJ, Klimyk AU (1991) Representation of Lie groups and special fucntions, vol 1. Kluwer Academic, Dordrecht
Voigt W (1928) Lehrbuch der Kristallphysik. Teubner-Verlag, Leipzig
Vollrath A (2006) Fast Fourier transforms on the rotation group and applications. Diploma thesis, Universität zu Lübeck
Watson GS (1969) Density estimation by orthogonal series. Ann Math Stat 40:1496–1498
Watson GS (1983) Statistics on spheres. Wiley, New York
Wenk HR (1985) Preferred orientation in deformed metals and rocks: an introduction to modern texture analysis. Academic, New York
Zuo L, Xu J, Liang, Z (1989) Average fourth-rank elastic tensors for textured polycrystalline aggregates without symmetry. J Appl Phys 66:2338–2341